Alneelain University
Graduate College
Department of Physics

Cu Doped ZnO as Transparent Electrode for Dye Sensitized Solar Cell (DSSC)

Khamael Ibrahim Abdulwahid

B.Sc. 2007

Supervised By

Dr. Musbah Hamed Babikier

2017 A.C. **1439 A.H.**

بِسْمِ اللَّهِ الرَّحْمَنِ
الرَّحِيمِ

يَرْفَعِ اللَّهُ الَّذِينَ آمَنُوا
مِنْكُم
وَ الَّذِينَ أُوتُوا
الْعِلْمَ دَرَجَات

صدق الله العلي العظيم
سورة المجادلة (11)

Dedication

To…. My Father…For attention and my mother...

For her endless giving

To… My husband, whom always supports me

To…. My Brothers and their children & My Sisters

and their children

To who supported me with their love, Attention

Kindness and Encouragement

ACKNOWLEDGEMENTS

First . I thank Allah for giving me power to complete the research.

Then :

To whom I had the light of life, to the man who encouraged me with all my life, to my beloved companion, to my love and my husband. I give you thanks and ask God to perpetuate a grace in my life..

I would like to express my deep thanks and gratitude to my supervisor Dr. Musbah Hamed Babikier for her great efforts.

I would also like to thank Mr.Abd alsakki suliman.

Also , I deeply thank all the staff of physics science Alneelain university.

Abstract

Pure and Cu doped ZnO nanoparticles, with different doping ratio (0, 2, 4, 6 and 8) at%, were prepared by hydro thermal method at 90 ^{o}C from zinc nitrate $Zn(NO_3)H_2O$ and sodium hydroxide NaOH as precursors, and with substitution additive of CuO as a dopant at the selected ratio.

The effect of Cu doping ratio on structural and optical properties for synthesized nanoparticles were studied by X-ray diffraction, UV-visible absorbance and Fourier transform infrared spectroscopy to find the optimum conditions for use the produced nanoparticles with iodine dye in solar cell application

X-ray diffraction measurements show polycrystalline structure for all samples identical with ZnO standard peaks. The crystallinety decrease with increasing doping ratio.

The non-uniform strain (ε), calculated by Williamson-Hall plot shows that the ε increase with increasing Cu ratio specially at 8%. The maximum value for crystalline size at 2% Cu then decreases with increasing doping ratio.

Optical properties showed that the transmittance increases with increasing doping ratio to 8% reaching values higher than 90% in the visible region. The energy gap was direct transition, and increasing of Cu content from 0 to 2% leads to decrease the optical band gap from 3.20 to 3.14 eV and then increase to 3.26 eV at 8% Cu due to decreasing the nanosize.

FTIR patterns show small peaks located in the range from 420 to 620 cm^{-1} corresponding to Zn-O vibrations, indicate on ZnO formation.

The I-V characteristics for DSSC under illumination , for samples based on Cu doped ZnO NPs with different ratio, show that the efficiency increase with increasing the Cu dopant ratio reach to 0.0439 at 8% Cu content.

الخلاصة

تم تحضير جسيمات اوكسيد الخارصين النانوية النقية والمشوبة بالنحاس وبنسب ذرية مختلفة (0 و 2 و 4 و 6 و 8) ٪ بالطريقة الحرارية المائية عند 90 °C من نترات الزنك H_2O (ZnNO3) وهيدروكسيد الصوديوم NaOH كمواد اولية، مع اضافة تعويضية من CuO وبالنسب المحددة.

تم دراسة تأثير نسبة التشويب بالنحاس على الخصائص الهيكلية والبصرية للجسيمات النانوية المحضرة، بواسطة حيود الأشعة السينية وامتصاص الأشعة فوق البنفسجية المرئية وتحويل فوريه للتحليل الطيفي للأشعة تحت الحمراء للعثور على الظروف المثلى لاستخدام جزيئات النانو المنتجة مع صبغة اليود في تطبيقات الخلايا الشمسية

أظهرت قياسات حيود الأشعة السينية تركيب متعدد التبلور لجميع العينات متطابقة مع قمم القياسية لأوكسيد الزنك. و انخفاض درجة التبلور مع زيادة نسبة التشويب.

الاجهاد الغير منتظم في الشبيكة (ε)، و المحسوب باستخدام معادلة ويليامسون-هول يدل على زيادة ε مع زيادة نسبة النحاس خاصة في 8٪. بينما كانت اكبر قيمة للحجم البلوري عند النحاس 2٪ ثم تنخفض مع زيادة نسبة التشويب.

أظهرت الخصائص البصرية أن النفاذية تزداد مع زيادة نسبة التشويب إلى 8٪ تصل إلى قيم أعلى من 90٪ في المنطقة المرئية. وكانت فجوة الطاقة ذات انتقال مباشر، وزيادة محتوى النحاس من 0 إلى 2٪ يؤدي إلى تقليل فجوة الطاقة البصرية من 3.20 إلى 3.14 فولت ومن ثم زيادة إلى 3.26 فولت عند 8٪ النحاس بسبب انخفاض الحجم النانوي.

بينت منحنيات FTIR قمم صغيرة تقع في نطاق 420-620 سم $^{-1}$ المقابلـــة للاهتزازات Zn-O، و التي تدل على تشكيل أكسيد الزنك.

بينت خصائص I-V لخلايا الصبغة DSSC تحت الإضاءة، للعينات المحضرة باستخدام عينات ZnO المشوب بالنحاس مع نسبة مختلفة، يدل على زيادة الكفاءة مع زيادة نسبة التشويب تصل إلى 0.0439% في محتوى النحاس 8٪

CONTENT

List of figures

Figure	Description
A	Absorbance
A	Area of the sample
a	Lattice Constant
c	Lattice Constant
d_{hkl}	Inter Planar Distance
D	grain size
E_c	Conduction Band Energy
E_F	Fermi Level Energy
E_p	Phonon Energy

List of Symbols

Symbol	Description
A	Absorbance
A	Area of the sample
a	Lattice Constant
c	Lattice Constant
d_{hkl}	Inter Planar Distance
D	grain size
E_c	Conduction Band Energy
E_F	Fermi Level Energy
E_p	Phonon Energy
E_v	Valence Band Energy
E_g^{opt}	Optical Energy Gap
FF	Fill factor
h	Blank Constant
$h\upsilon$	Photon Energy
I_{sc}	Short circuit current
J	Current Density
k_B	Boltzmann's Constant
n_e	Electrons Concentration
n_i	Intrinsic Carrier Concentration
P	Holes Concentration
e	Charge of Electron
R	Resistance
T	Temperature
T	Transmittance
t	Film Thickness
V_{oc}	Open circuit voltage
ρ	Resistivity
α	Absorption Coefficient
θ	Diffraction angle
η	Efficiency

List of Abbreviations

Abbreviations	Description
AFM	Atomic Force Microscope
C.B.	Conduction Band
FWHM	Full Width at Half Maximum
FTIR	Fourier Transform Infra-Red
I-V	Current-Voltage
IR	Infrared
I	The current
I_d	Dark current
I_{ph}	Photo current
I_n	Noise current
SEM	Scanning Electron Microscopy
UV	Ultra Violet Spectrum
XRD	X-Ray Diffraction

CHAPTER ONE

INTRODUCTION & BASIC CONCEPT

1-1 Introduction

Zinc oxide is a very promising material in many applications because it possesses a wide range of useful properties. It is widely used as an additive to many products including plastics, ceramics, glass, cement, rubber, coatings, ointments, food, etc. Due its high transparency, recently ZnO has drown significant attention in the field of Dye Sensitized Solar Cell fabrication. Where, many researchers suggested that the ZnO is very promising when used as electrode.

ZnO is inherently n-type semiconductor ,howevere, p-type ZnO is rather difficult to be achieved . therefore, major efforts have been focused to overcame this problem . many dopant has been suggested to modulate the conductivity type in ZnO. One of these is the copper where the previous work showed that the cu – doped ZnO emits green light with very high intensity compared to the other regions in the visible spectrum these results motivate us to fabricate DSSC based CU-Doped ZnO.

The use of ZnO in DSSC is promising due to the electronic properties of this oxide. Electron mobility and diffusion coefficient in ZnO is much higher than that in TiO2. These properties are profitable for DSSCs application because they support fast charge transport and electron recombination reduction. Moreover, the crystallization and anisotropic growth of ZnO crystal is relatively easy and allows the preparation of structures with various structural shapes

1-5 Aim of the Work

Synthesis pure and Cu doped ZnO nanoparticles with different doping ratio and characterized their structural and optical properties to use these

nanoparticles, with iodine, to fabricate dye-sensitized solar cell with good parameters.

1-3Thesis structure

This work consist of five chapters, the first chapter covers the general introduction and guide for the research. The second chapter presents the basic concepts of ZnO properties and the basic concepts of DSSC. The materials synthesis methods is introduced in the third chapter. Also the principles of the characterization techniques is covered briefly. The results and the discussion are presented in chapter four. Finally, the important achievements were summarized in the conclusion part

CHAPTER TWO

THEORETICAL PART

2-1 Introduction

The high attention for renewable energy sources and the increases in the cost of oil have compelled many countries to search for low cost energy sources and technologies, such as solar cells [1].

A dye-sensitized solar cell (DSSC) is a low-cost solar cell belonging to the group of thin film solar cells [2]. It is based on a semiconductor formed between a photo-sensitized anode and an electrolyte. It was originally invented in 1988 by Brian O'Regan and Michael Grätzel at UC Berkeley, and this work was later developed by them until the publication of the first high efficiency DSSC in 1991 [3].

Dye sensitized solar cell (DSSC) is the only solar cell that can offer both the flexibility and transparency. Its efficiency is comparable to amorphous silicon solar cells but with a much lower cost [4]. It is simple to make using printing techniques [5].

Although its conversion efficiency is less than the best thin-film cells, in theory its price/performance ratio should be good enough to allow them to compete with fossil fuel electrical generation [6].

In a traditional solid-state semiconductor, a solar cell is made from two doped crystals, one doped with n-type impurities, and the other doped with p-type impurities. When placed in contact, some of the electrons in the n-type portion flow into the p-type to fill in the holes, and align the Fermi levels of the two materials, cause depleted region. This transfer of electrons produces a potential barrier [1].

Photons of the sunlight can excite electrons on the p-type side by provide enough energy to push an electron out of the lower-energy valence

band into the higher-energy conduction band. Electrons in the conduction band are free to move out of the p-type side into the n-type side, and flow throw the load and then flow back into the p-type material where they recombine with the valence-band holes [7]

Illuminated organic dyes can generate electricity at oxide electrodes in electrochemical cells [8]. The main challenge in dye solar cell its instability and its efficiency. The efficiency improved by optimizing the porosity of the electrode prepared from nanoparticles oxide powder. A modern DSSC is composed of a porous layer of metal oxide nanoparticles, covered with a molecular dye that absorbs sunlight. The metal oxide is immersed under an electrolyte solution, above which is a platinum-based catalyst [9].

Sunlight passes through the transparent electrode top contact into the dye layer on the surface of the ZnO with enough energy, from which an electron can be injected directly into the conduction band of the ZnO. The electrons flow toward the transparent electrode where they are collected for powering a load. After flowing through the external circuit, they are re-introduced into the cell on a metal electrode on the back, flowing into the electrolyte. The electrolyte then transports the electrons back to the dye molecules.

1-4 Literature survey

M. Mukhtar et al.,(2012) [10] have synthesized nanocrystalline Cu-doped ZnO particles by co- precipitation method. The composition, structural, optical and magnetic characterizations were performed by EDX, XRD and UV-Visible spectrometer. The results confirmed that nanocrystalline Cu-doped ZnO particles have a hexagonal wurtzite structure with a high degree of crystallization and a crystallite size of 10 - 16 nm. For Cu above 11 at%, the

X-Ray diffraction pattern possessed CuO secondary phase which shows the solubility limit of Cu in the ZnO lattice.

C. Bhakat et al.,(2012) [11] have synthesized hexagonal shape zinc oxide nanorods by thermal decomposition process by wet chemical method, using zinc chloride (ZnCl2) as precursor with sodium hydroxide (NaOH) in 1:2 molar ratios by the. The sample was characterized by UV-Vis spectrophotometer, XRD and SEM. Further its application in solar cell. The results indicate that the as-prepared ZnO Nano-rods are uniform with diameters of 100–200 nm and lengths of about 1μm.

C. Justin et al.,(2013) [12] have synthesized Mg doped ZnO like root for used in photo anode with high electron transport and improved light efficiency of dye-sensitized solar cells (DSSC). DSSC based on a 5 mol % Mg-doped ZnO electrode of low thickness ~4 μm, gained an improved short-circuit current density of 9.98 mAcm−2, open-circuit photo voltage of 0.71 V, fill factor of 0.58, and overall conversion efficiency of 4.11% under 1 sun illumination.

C. Hsu et al.,(2014) [13] have studied the characteristics of dye-sensitized solar cells (DSSCs) with graphene/ZnO nanoparticle bilayer structure. The enhancement of the performance of DSSCs achieved using graphene/ZnO nanoparticle films is attributable to the introduction of an electron-extraction layer and absorption of light in the visible range and especially in the range 300–420 nm. DSSC that was fabricated with graphene/ZnO nanoparticle film composite photoanodes exhibited a Voc of 0.5V, a Jsc of 17.5 mA/cm2, an FF of 0.456, and a calculated η of 3.98%.

J. Tamil et al.,(2014) [14]have synthesized Zinc oxide nanoparticles by wet chemical method using Zinc acetate dihydrate and potassium hydroxide

as a precursor materials. Ethanol was used as a solvent at room. The sample were characterized by field emission scanning electron microscopy (FE-SEM), transmission electron microscopy (TEM), X-ray diffraction (XRD), ultraviolet visible spectroscopy (UV-Vis) and photoluminescence spectroscopy (PL). The TEM images showed that the average size of the nanoparticles was calculated to be ~33nm. Photoluminescence (PL) studies show bright luminescence with peak maximum at 540nm and 563nm. The optical transmission spectrum of colloidal nanoparticles of ZnO shows sharp absorption at 4.2eV which is blue shifted as compared to bulk ZnO (3.36eV).

M. Jyoti et al.,(2015) [15] have synthesized zinc oxide nanostructures, for Biomedical application, by using zinc chloride and sodium hydroxide as the precursors at different temperatures. The ZnO nanostructures obtained were characterized by XRD, SEM and EDX. The ZnO powders have hexagonal wurtzite structure and nanometric-sized crystallites. The size of the particle increases as the reaction temperature is increased.

D. Ahmed et al.,(2015) [16] have prepared zinc oxide nanoparticles via hydrothermal growth using zinc acetate dihydrate and sodium hydroxide. Crystal structure and morphological features of the obtained ZnO nanoparticles were characterized by XRD and SEM. The results obtained show that this hydrothermal synthetic method can produce good quality ZnO nanoparticles.

N. Salahuddin et al.,(2015) [17] studied the effects of annealing temperatures on zinc oxide nanoparticle size synthesized via precipitation method. The structure and composition of the precursor and prepared ZnO NPs were studied using XRD, UV-visible spectroscopy, SEM, TEM and FTIR. The XRD results revealed that the ZnO NPs are highly crystalline,

having the hexagonal wurtzite crystal structure. The SEM images showed that ZnO nanoparticles prepared in this study were spherical in shape. The results of the UV-Vis studies showed that the optical properties of the ZnO NPs depended on the annealing temperature. The size of ZnO NPs increased with an increase in annealing temperature.

R. Sadraei (2016) [18] have synthesized ZnO nanoparticles by simple method of precipitation sounds using ZnSO4 and NH4OH as precursors. The synthesized ZnO NPs were characterized by XRD, SEM and EDX. According William-Hal method, the mean size of particles was achieved equal to 30 nm. SEM analysis revealed that the morphology of ZnO nanoparticles to be flake like shapes with the mean particle size of 30 nm. Finally, the analysis of the synthesized nano sample by using EDX has indicated that the purity of ZnO was quite high.

2-2 Some of ZnO Chemical and physical properties

Zinc (ZnO) is white solid powder. It is one of (II-VI) semiconductor compounds, do not dissolve in water, 81.38 g /mole molecular weight and 5.607 gm/cm^3 density [19] sublimate by heating without dissociation [20]. The zinc blend and the Wurtzite Structure are formed. The crystalline network of zinc oxide (ZnO) consists of oxygen and zinc atoms with tetrahedral (for zinc blend) or hexagonal structure (Wurtzite), the second structure is more stable which shown in Fig. (2-1) with crystal dimensions a = 3.2490 Å c = 5.2070 Å [21]. Table (2.1) shows some physical properties of zinc oxide with crystalline formation

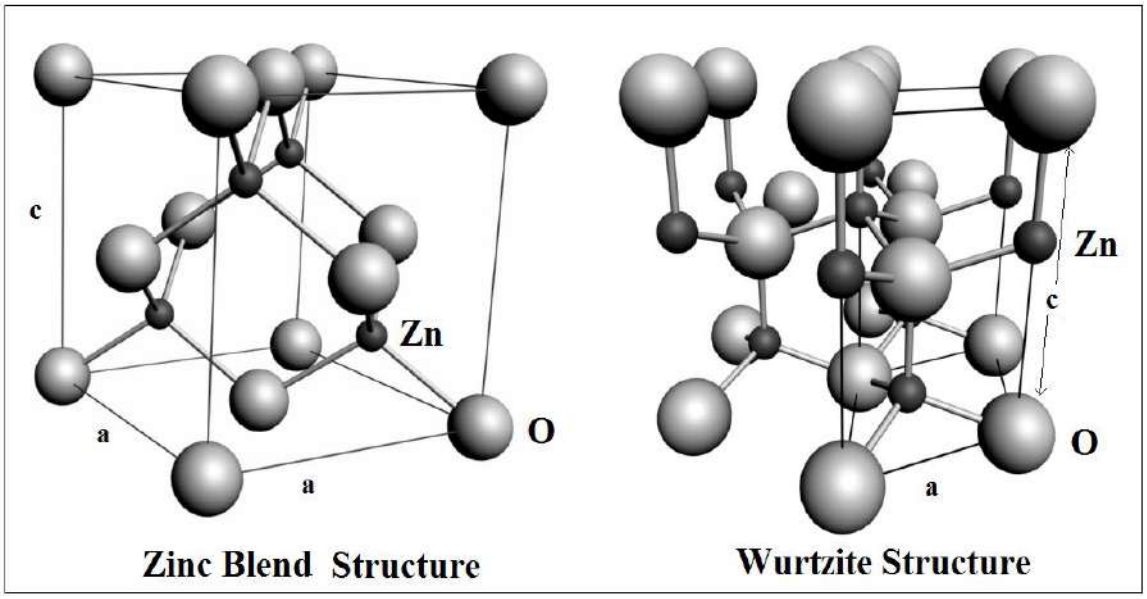

Fig. 2-1: Crystalline structure of zinc oxides (Wurtzite and zincblend) [22]

Table (2-1) Characteristics of ZnO Zinc Oxide [23] **(Wurtzite)**

Property	**Value**
Lattice parameters at 27˚C	a=3.2495 Å ; c=5.2069 Å
Density	gm/cm^{3}5.607
Melting point	1975˚C
Thermal Conductivity	100 mW/cm K at 27˚C
Static dielectric constant	8.656
Refractive index	2.008
Energy gap	3.4 eV(direct)
Intrinsic carrier Concentration	10^6 cm^{-3}< n<10^{20} cm^{-3}
Exciton binding energy	60 meV
Electron effective mass	0.24
Electron Hall mobility at 27˚C	200 cm^2/Vs

2-3 Some applications of zinc oxide

Zinc oxide is a very promising material in many applications because it possesses a wide range of useful properties. It is widely used as an additive to many products including plastics, ceramics, glass, cement, rubber, coatings, ointments, food, etc. .

ZnO has a wide power gap of up to 3.2-3.3VV electron-volt at room temperature [19] and high transparency in the visible area, which can be used in some photovoltaic applications such as light emitting diodes, laser diodes, optical sensors and solar cell. It is an alternative to ITO as a transparent conductive oxide. Zinc oxide also has significant piezoelectric properties that make it suitable for acoustic wave devices [24] . Zinc oxide has recently been used in ultraviolet lamps [25]. In addition, zinc oxide is a vital safety that attracts to use it for chemical sensing, especially in medical applications [26] and as antimicrobial agents [27]. Moreover, doping with many transitional metals can alter its properties.

Zinc oxide can be formed to be nanoparticles and in various forms such as nano-rods, nanowires, nano-belts and nano-tetrapods which depend on the method of preparation [28]thus enabling it to be used in many applications in many industrial, military and medical fields [29].

ZnO nano particles can be obtained with a variety of particle structures, which its use in a wide range of applications. Therefore the development of a method of synthesizing crystalline zinc oxide has become more interested in many researches [30].

Technology for using nanoparticles of oxide materials are currently among the most developing scientific and technologies. The use of nanoparticles of oxide materials can used in ceramics, optical filters and ultraviolet radiation, and catalysts. These materials are also useful in biomedical researches [31].

Metal oxide nanoparticles, combined with other materials, provide possibilities for obtaining improved chemical, mechanical, optical or electrical properties.

Fig. (2-2) shows the schematic representation of the main application fields for zinc oxide.

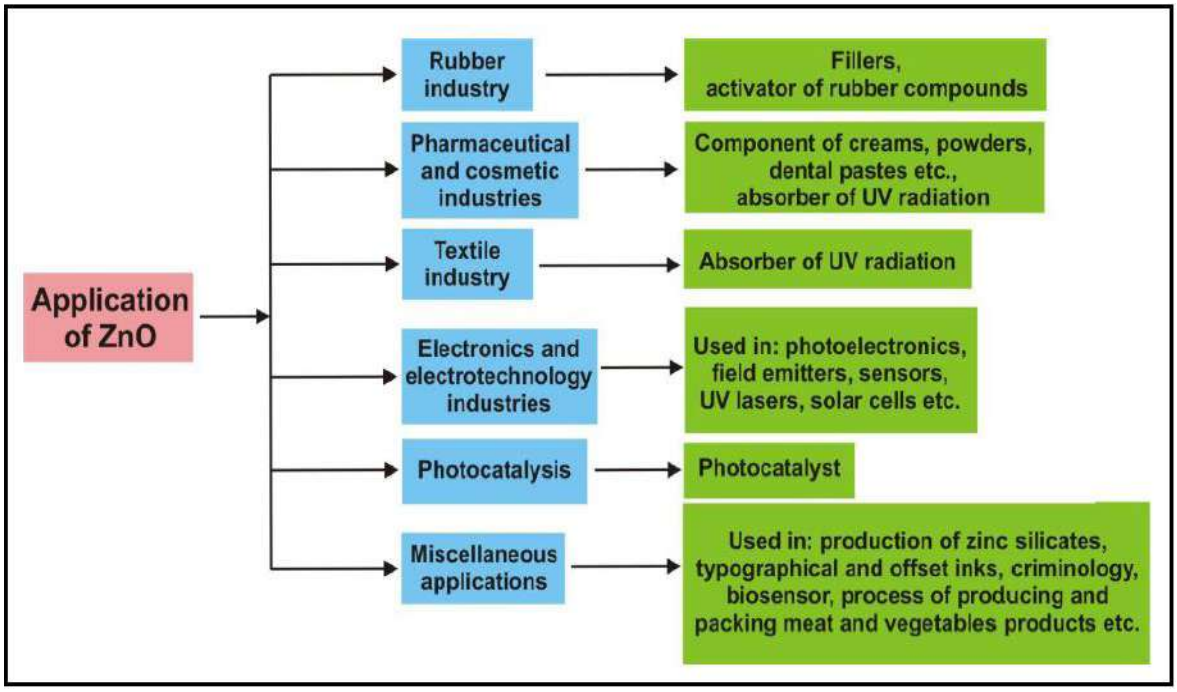

Fig. 2-2 :Schematic representation for ZnO application [30].

The use of ZnO in DSSC is promising due to the electronic properties of this oxide. Electron mobility and diffusion coefficient in ZnO is much higher than that in TiO_2. These properties are profitable for DSSCs application because they support fast charge transport and electron recombination reduction. Moreover, the crystallization and anisotropic growth of ZnO crystal is relatively easy and allows the preparation of structures with various structural shapes [32].

2-4 Nanotechnology

Nanotechnology, is the development of materials or species with low scales between 1 to 100 nm and study the materials properties at the nano-scale and their structures using special devices and systems. It has been used

in many important scientific fields such as in electronic devices, biology and medicine. This technology, which is at the scale of the building blocks of the cell, permit to smaller and more efficient devices [33]. There are two distinct approaches to the fabrication of nanostructures: the top-down approach and the bottom-up approach [34].

2-4-1 Preparation of Nanoparticles

Nanoparticles generation divided into four general methods:

- Wet chemical synthesis route include: sol–gel process, hydrothermal techniques and precipitation methods.
- Mechanical preparation techniques include grinding, ball milling and mechanical alloying techniques.
- Form-in-place methods include lithography, vacuum deposition techniques like CVD, PVD and spray coatings.
- Gas phase synthesis includes flame pyrolysis, electro-explosion, laser ablation, high temperature evaporation and plasma synthesis.

Wet chemical synthesis has been widely used in different theses due to its simplicity, low cost, large scale production at low temperature growth. In order to get the product of oxides, this method involves precipitation of hydroxides, chlorides, sulfates, carbonates and oxalates by the addition of base solution to the raw material followed by calcination [35].

In this experimental work, chemical precipitation method was adopted to synthesize Zinc Oxide and Copper doped Zinc Oxide.

2-5 Structural properties

The knowledge of Structural properties is very impotant to understand its crystallinety and phases, which effect on other physical properties.

William Lawrence Bragg in 1913 show that the incident X-rays at certain specific wavelengths and incident angles on crystalline solids are

produced patterns with intense peaks of reflected radiation depend on inter-atomic distances, i.e. it is a good probe for this length scale. According to deviation angle (2θ), the phase shift causes constructive interferences if the phase shift is a multiple of 2π (path difference equal to multiple of wavelength as shown in Fig. 2-3) this condition can be expressed by Bragg's law [36]

$$m\,\lambda = 2\,d_{hkl}\,\sin\Theta \qquad \text{.....(2-1)}$$

where λ, Θ and m represent X-ray wavelength (λ =1.5406 Å for Cu target), diffraction angle and diffraction order respectively.

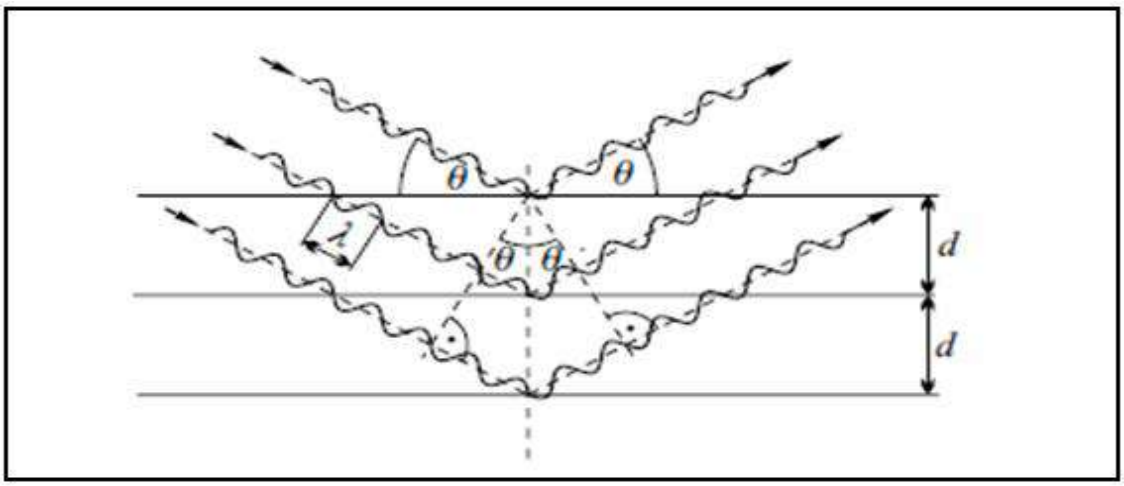

Fig. 2-3: Reflection of X-ray beam from a set of atomic planes separated by *d* [36].

The average nanocrystalline size was calculated using Debye-Scherrer's formula[37]:

$$D = \frac{K\lambda}{\beta_{hkl}\cos\theta} \qquad \text{.....(2-2)}$$

where D = crystalline size, K = shape factor (0.9).

The strain induced in powders due to crystal imperfection and distortion was calculated using the formula:

$$\varepsilon = \frac{\beta_{hkl}}{4\tan\theta} \qquad \text{.....(2-3)}$$

From equations (2-2 and 2-3), it was confirmed that the peak width from crystallite size varies as 1/cosθ, while the strain varies as tanθ. Assuming that the particle size and strain contributions to line broadening are independent to each other and both have a Cauchy-like profile, the observed line breadth is simply the sum of contribution of the two effects.

$$\beta_{hkl} = \frac{K\lambda}{D\,Cos\theta} + 4\varepsilon\,tan\theta \qquad \text{.....(2-4)}$$

By rearranging the above equation, we get

$$\beta_{hkl}Cos\theta = \frac{K\lambda}{D} + 4\varepsilon\,sin\theta \qquad \text{.....(2-5)}$$

The above equation called W-H equations. A plot is drawn between $\beta_{hkl}\cos\theta$ (along the y-axis) against $4\sin\theta$ (along the x-axis). The crystalline size was estimated from the y- intersection, and the strain (ε) from the slope of the best fit line. This equation assumed that the strain be uniform in all crystallographic directions, thus considering the isotropic nature of the crystal, where the material properties are independent on the directions along which they are measured.

2-6 Optical Properties of Semiconductors

The absorption spectrum demonstrates a useful information about the semiconductors materials, such as the type of transition, energy gap (Eg), permittivity and other optical properties [38].

2-6-1 Optical Absorption and Absorption Edge

When a semiconductor is illuminated with light, the photons may be absorbed through the semiconductor, depending on the photon energy (hυ); where h is Plank's constant υ is the incident photon frequency, and the electronic transition between the valance band (V.B.) and the conduction band (C.B.) in the crystal start at the absorption edge which corresponds to the minimum energy difference between the lowest minimum of the C.B. and the

highest of the V.B. i.e. the E_g [39, 40]. If hυ≥ Eg the photon can interact with a valence electron, elevates the electron into the C.B. and creates an electron-hole pair. The minimum wavelength (λ) of the incident photon which creates the electron-hole pair is defined as [41].

$\lambda = hc / E_g$ or $\lambda(nm) = 1240 / E_g$ (eV) ……..…….. (2-6)

The intensity of the photon flux decreases exponentially with distance (t) through the semiconductor according to the beer-Lambert equation [42].

$$I = I_o e^{-\alpha t} \quad \text{……..……(2-7)}$$

Where I_o and I are the incident and the transmitted photon intensity respectively and α is the absorption coefficient, which is defined as the relative number of the photons absorbed per unit distance of a semiconductor, and t is the thickness of the material [43, 44].

2-6-2 Optical Transition

The electron transitions between the V.B. and the C.B. are divided into direct and indirect [45] it is obeying the following Tauc equation:

$$\alpha h\upsilon = B\,(h\upsilon - Eg)^r \quad \text{……..(2-8)}$$

where B is a constant inversely proportional to amorphousity, r=1/2, 3/2, 2, 3 for allowed direct, forbidden direct, allowed indirect, forbidden indirect transitions respectively.

Direct transitions in general occur between the initial and the final states of the same wave vector value of electron occurs, Δk = 0 for conservation momentum. The absorption coefficient for this transition takes the values from 10^4 to 10^5 cm^{-1}. This transition takes place in crystalline and polycrystalline semiconductors. Allowed direct transition occurs when an

electron makes direct transition from the top of the V.B. to the bottom of the C.B. and the wave vectors of initial and final states are equal to zero as shown in Fig. (2-4 a) [46]. Forbidden direct transition occurs between the state of the same wave vector but the wave vector does not equal zero, i.e. the allowable transition occur at different positions of C.B. and V.B. [46], as shown in Fig. (2-4 b)

Indirect transitions occur when the C.B. minima are not at the same value of the k as the V.B. maxima, the assistance of phonon is necessary to conserve the crystal momentum, therefore $h\upsilon=E_g \pm E_p$ where E_p is the emitted or absorbed phonon energy [47], α takes the values 1 to 10 cm^{-1}. Allowed indirect transitions occur from the top of the V.B. to the bottom of the C.B [48] as shown in figure (2-4 c) forbidden indirect transitions occur from any point that the top of V.B. to any point other than the bottom of the C.B., as shown in figure (2-4 d)

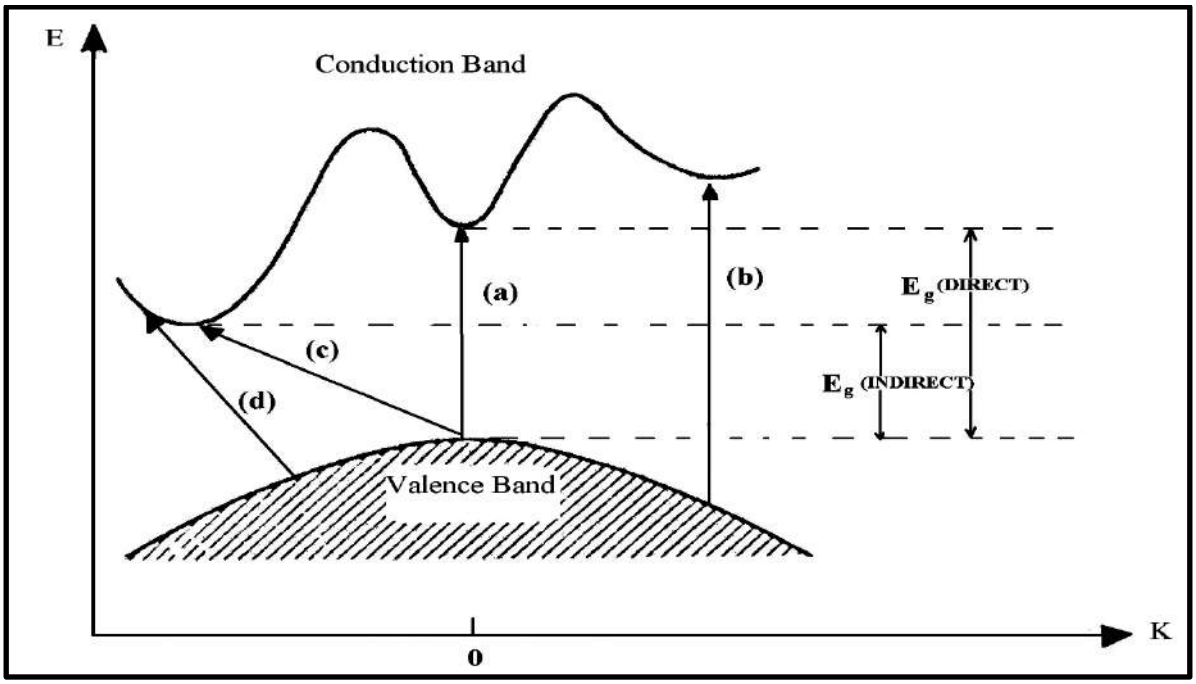

Fig.(2-4): The optical transitions (a) Allowed direct, (b) Forbidden direct, (c) Allowed indirect, (d) Forbidden indirect [47].

2-6-3 Optical Constants

The interaction between electromagnetic radiation with semiconductor is characterized by optical constants: refractive index (n), the extinction coefficient (k) and the real and imaginary parts of dielectric constant [49]. A detailed measurement of the values and variable of the optical constant over some range of energy provides information on such fundamental properties as the band structure of the material or the impurities in crystals. Detailed and accurate knowledge of the optical constant is also required in such practical applications as the design of lens system, fiber optics, and second harmonic generation [50].

The following relation which expresses the idea that all the incident power is either, reflected, absorbed or transmitted and can be utilized [51].

$R+A+T=1$ …… (2-9)

The refractive index value (n) can be calculated from the formula [52]

$$n=\left(\frac{4R}{(R-1)^2}-k^2\right)^{\frac{1}{2}}-\frac{(R+1)}{(R-1)} \quad \text{…….... (2-10)}$$

The extinction coefficient is related to the absorption coefficient α by the relation [53]

$k = \alpha\lambda / 4\pi$ ……. (2-11)

The real ε_r and imaginary ε_i parts of dielectric constant can be calculated as follows [54]

Complex refractive index $N^* = n - ik$ ……. (2-12)

Complex dielectric constant $\varepsilon^* = \varepsilon_r - i\varepsilon_i$ …..……..…….. (2-13)

From the relation $N^* = \sqrt{\in *}$, therefore:

$\varepsilon_r = n^2 - k^2$ ……..……..... (2-14)

$\varepsilon_i = 2nk$ ..... (2-15)

2-7 Fourier Transform Infra-Red Spectroscopy

The principle of FTIR spectrometer based on the Michelson interferometer, which consists basically of a beam splitter and two flat mirrors. One of the mirrors is fixed in one interferometer arm; the other is movable in the second interferometer arm [55].

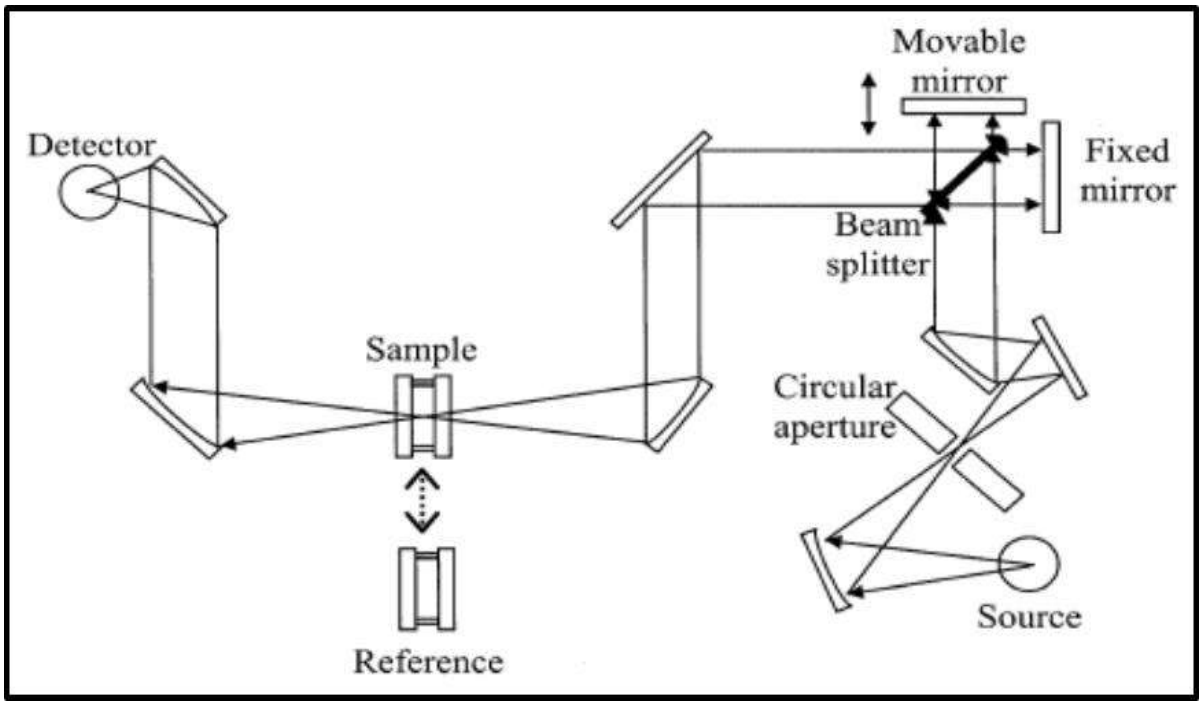

Fig. 2-5: Diagram of FTIR spectrometer with Michelson Interferometer [55]**.**

The spectrum can be reconstructed using a Fourier transform of the temporal coherence of signal measurements at many discrete positions of the moving mirror. It is capable to detect spectral with high resolution.

The mathematical procedure, which is employed to convert the IR interferogram (intensity versus time, also called time domain) to an IR spectrum (intensity versus frequency, also called frequency domain) is called Fourier transformation. Sample and reference interferograms are separately

transformed. After wards the ratio of both is automatically calculated and displayed as instrument-independent IR transmission spectrum [56].

2-9 Solar cell

A solar cell is a device that converts the energy of sunlight directly into electricity by the photovoltaic effect. Photovoltaic is the field of technology and research related to the application of solar cells in producing electricity for practical use[57] .

A solar cell under illumination is characterized by many parameters:

- **Short–Circuit Current** (I_{sc}) is the current in the illumination device at 0 volt bias.
- **Open–Circuit Voltage** (V_{oc}) the bias applied on device to decimate the current generated by illumination (I= 0 A) [58]**.**
- **Fill Factor** (FF). is the ratio of the available power at the maximum power point (P_m) divided by the open circuit voltage (V_{OC}) and the short circuit current (I_{SC}) [59]

$$FF = \frac{P_m}{V_{OC} \times I_{SC}} \qquad \text{.....(2-16)}$$

The fill factor is increased by increasing the shunt resistance (R_{sh}) and decreasing the series resistance (R_s)

- **Efficiency (**η) is the power density delivered at operating point of the incident light power as a fraction of the incident light power density, which is given by [59].

$$\eta = \frac{J_{max} V_{max}}{p_{in}} \times 100\% \qquad \text{.....(2–17)}$$

Efficiency is related to J_{sc} and V_{oc} using FF,

$$\eta = \frac{j_{sc} V_{oc} FF}{p_{in}} \times 100\% \quad \text{.....(2–18)}$$

These four quantities: Jsc, V_{oc}, FF and η are the key performance characteristics of a solar cell. All of these should be defined for particular illumination conditions.

Fig. (2-6) shows parameters are indicated on a current – voltage curve of a solar cell under illumination [58].

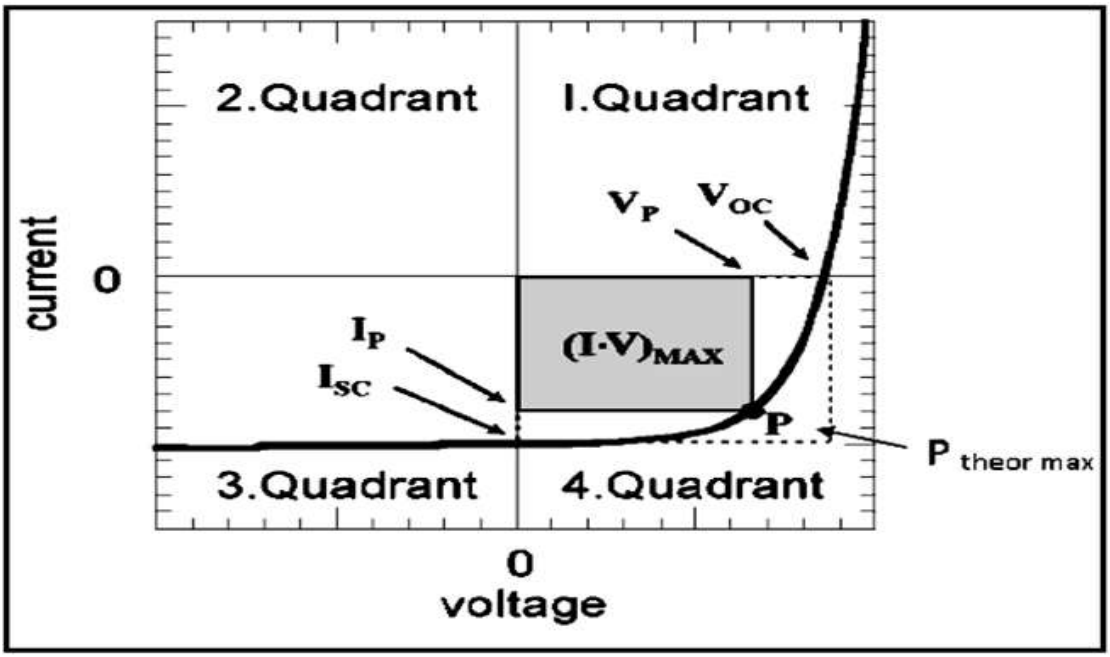

Fig. 2-6: solar cell parameters under illumination at I-V curve [58]

To understand the electronic behavior of a solar cell it is useful to create electrically equivalent circuit. No solar cell is ideal, so a shunt resistance and a series resistance component are added to the model. The resulting equivalent circuit of a solar cell is shown in Fig. (2-7)

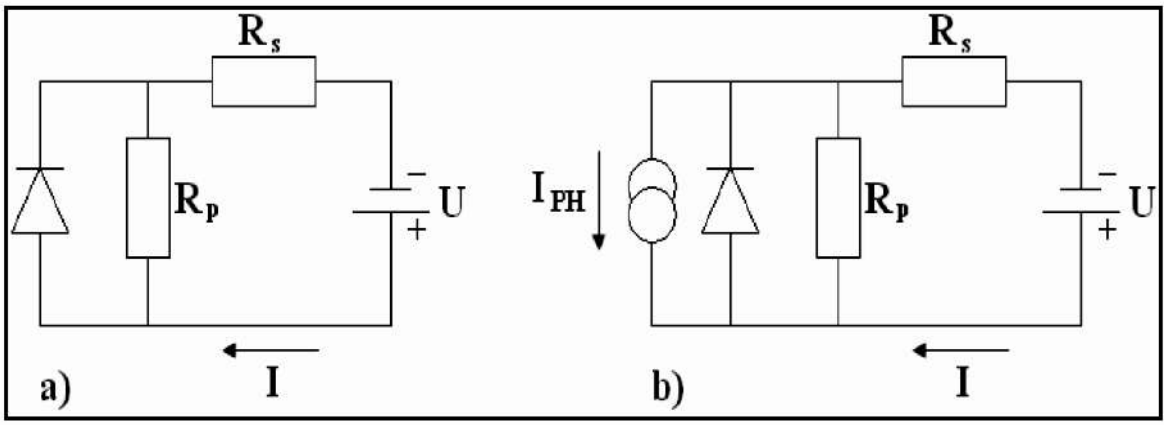

Fig. 2-7: Equivalent circuit for a stander solar cell (a)in the dark (b)under illumination [60]**.**

CHAPTER THREE

EXPERIMENTAL PART

3-1 Introduction

This chapter includes the experimental processes used to fabricate the pure and Cu doped ZnO nanoparticles with different doping ratio and techniques used to examine these nanoparticles. Finally the steps for fabricated solar cell based on iodine dye and the fabricated nanoparticles. Also it includes photovoltaic measurements which are presented by current-voltage characteristics of dye-sensitized solar cell (DSSC).

3-2 Reactants

Zinc nitrate $Zn(NO_3)H_2O$ (as a zinc source) and sodium hydroxide (NaOH) were used as precursors for the formation of the zinc oxide and copper oxide as dopant. Distilled water was used as solvent.

3-3 Nano Particles Preparation

Pure and Cu doped ZnO nanoparticles samples were prepared by hydro thermal method. Zinc nitrate $Zn(NO_3)H_2O$ and sodium hydroxide NaOH were dissolved in distilled water at room temperature with ratio of 1:1 ($Zn(NO_3)H_2O$: NaOH), by stirring for complete dissolution (forming transparent white solutions), to form the liquid media of the desired concentrations of 0.1M, then inserted into an electrical oven at 90°C for 8 hours. These solutions were reacted to produce zinc oxide precipitates. Following the precipitation, the solution was centrifuged at 3000 rpm for two hours. Then the ZnO nanoparticles was dried by heating at 60°C for 10 hours. This experiment was repeated five times but with substitution additive of CuO with $Zn(NO_3)H_2O$, as a Cu dopant at different concentration (0, 2, 4, 6and 8) at%.

In this process, the reaction of Zn^{2+} ions and sodium nitrate proceeds as shown in the following equations:

$$Zn(NO_3)_2 + 2NaOH \xrightarrow{\Delta} Zn(OH)_2 + 2NaNO_3 \quad \text{…..……(3-1)}$$

$$Zn(OH)_2 + 2NaNO_3 \xrightarrow{\Delta} Zn(OH)_2 \quad \text{……..……..(3-2)}$$

$$Zn(OH)_2 \xrightarrow{\Delta} ZnO + H_2O \quad \text{……..……(3-3)}$$

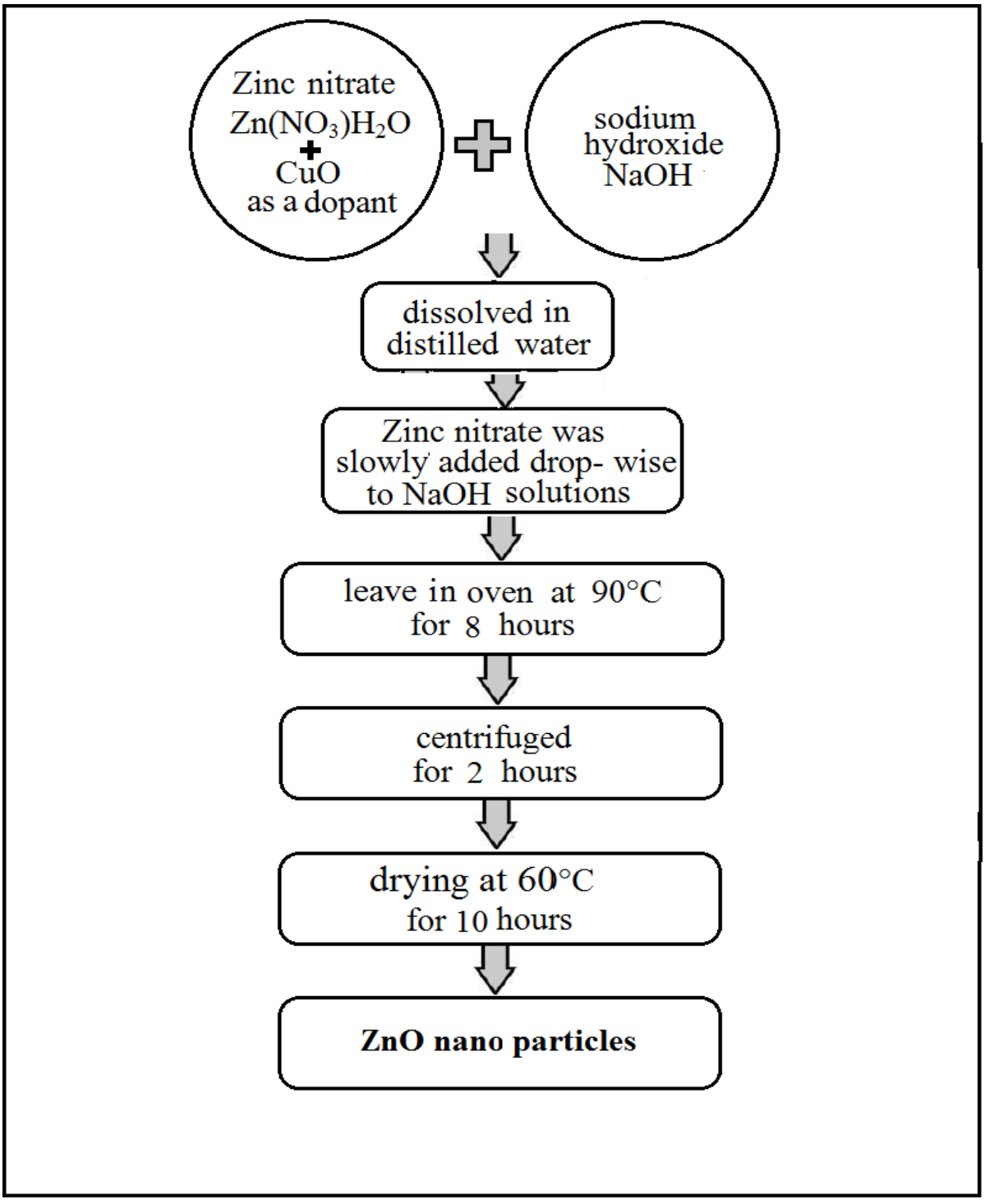

Fig. 3.1: Preparation process of Cu doped zinc oxide nanoparticles

3-4 Nanoparticles Examination

The prepared nanoparticles were examined by different techniques to study their structural, optical and electrical properties. .

3-4-1 X-Ray Diffraction

The structure of deposited thin film has been analysis using X–ray diffraction system type Bruker. The source of radiation was Cu (K_α) with wavelength λ= 1.5405 Å, the current was 30.0 mA and the voltage was 40 kV. The scanning angle 2θ (5˚-80̊) with speed of 5.00 (degree /min) and preset time = 0.24 s.

3-4-2 VU-visible Spectroscopy

The optical properties of pure and Cu doped ZnO nanoparticles suspended in water have been examined by UV-Visible spectrometer (UV mini1240 SHIMADZU SED SPEC -48), in the wavelength ranged from (300-900) nm. This spectrometer contains two light sources Deuterium and Tungsten lamp. This apparatus is of the double beam type, one of them passes through suspension in quartz cell, while the other passes through quartz cell filled with ethanol. The method of measurement depends on the transmission through the sample.

3-4-3 FTIR Measurements

Fourier-transformed Infra-red spectrum (FTIR) for pure and Cu doped ZnO nanoparticles, prepared with different doping ratio, were measured by (*satellite FTIR thermo matson*) over the range of 400-4000 cm^{-1} with resolution 4 cm^{-1} in the transmittance mode.

3-5 Solar cell fabrication

The cell has 3 primary parts. On top is a transparent anode made of fluorine tin dioxide (FTO) deposited on glass substrate. The substrates were first cleaned successively in Acetone Ethanol and DI water for 10 min in each step and then dried . On the back of this conductive plate, thin layer of zinc oxide or Cu doped zinc oxide was deposited with highly porous structure by doctor blade technique then by sintering as follows:

0.2 g of ZnO, 4 g of terpineol and 4 mL of ethanol were mixed together . Ethylcellulose solution in ethanol then was added into ZnO solution. Ethanol and water were subsequently removed from the solution in a rotary-evaporator at an initial temperature of 60 °C in order to create a viscous paste.

The photoelectrodes were prepared by spreading the paste on FTO glass substrate. The FTO glass substrates were cleaned with soap and rinsed with distilled water. They were then treated in acetone in an ultrasonic bath in ethanol for 5 min. The substrates were dried and placed in furnace at 400°C for 30 min.

A layer of oxide paste was spread on the FTO glass substrates by the doctor blading technique, relaxed under an ethanol atmosphere for at least 5 minutes and dried at RT for 5 min. The films were then annealed at 400°C for 30 min.

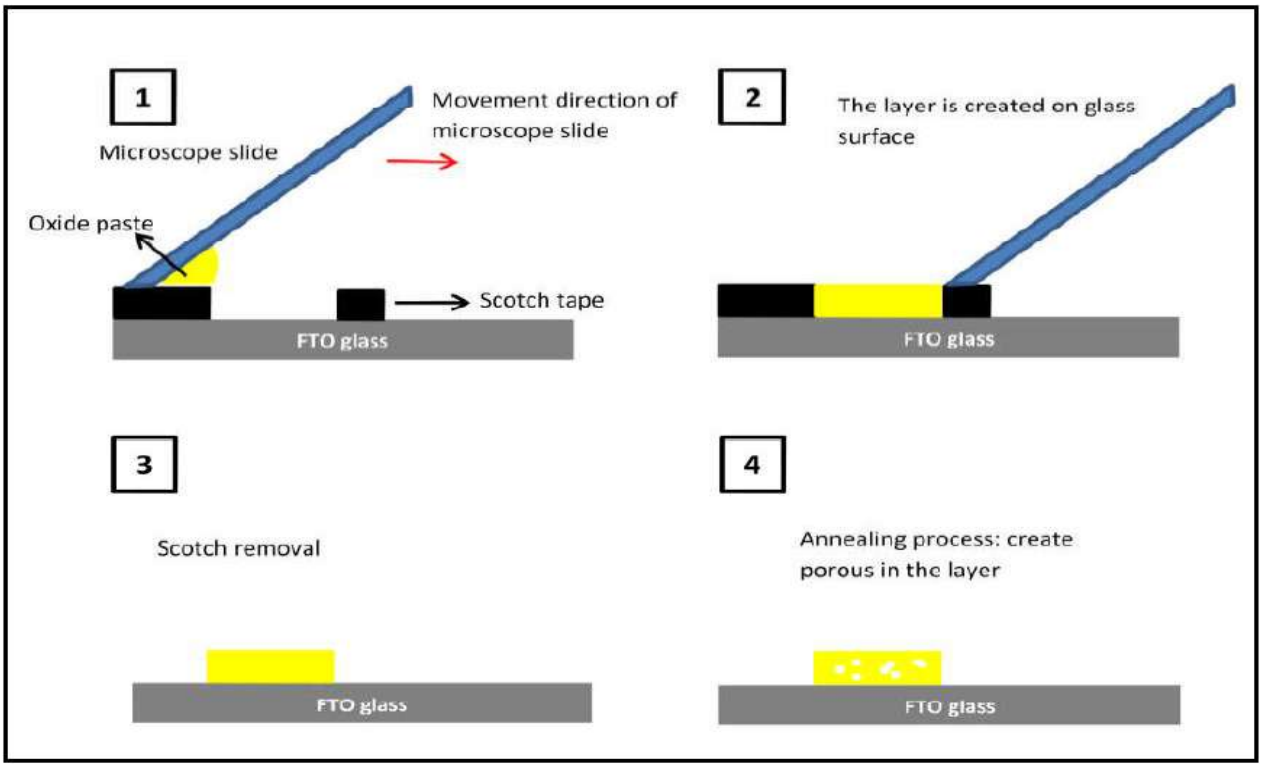

Fig. 3-2: Scheme of doctor blade technique layer deposition

A separate plate is then made with a thin layer of the iodide electrolyte spread over a conductive sheet, typically Graphite layer. The two plates are then joined and sealed together. This constriction has a number of advanced compared to the silicon cells because they require no expensive manufacturing steps.

3-6 Current –Voltage Characteristics

The electrical measurements for DSSC based on ZnO nanoparticles, which was prepared with different Cu doping ratio, include current-voltage characteristic measurements in the dark condition and under illumination (when they were exposed to Halogen lamp light with intensities (550) mW/cm^2), by using keithley digital electrometer 616, voltmeter and D.C. power supply as shown in Fig. (3-7). The bias voltage was varied over the range of 0 – 1 Volt in the case of forward and reverse bias.

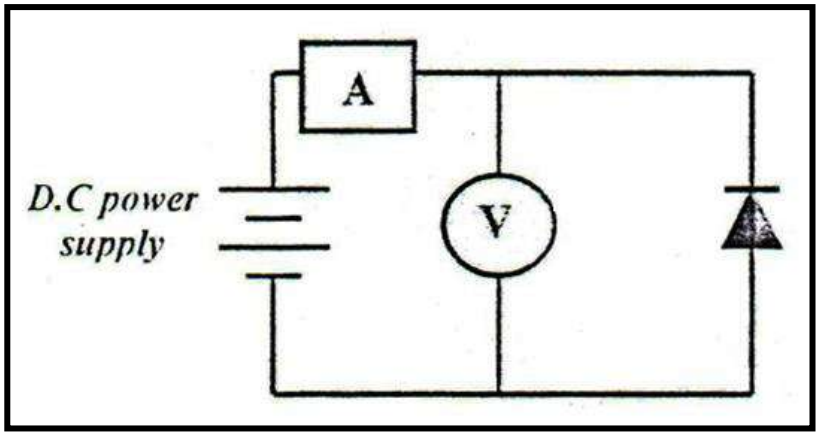

Fig. 3-3: Circuit diagram for I-V measurement of DSSC solar cell

where V is the forward bias voltage, I_f is the forward bias current.

The other solar cell parameters were determined from the I-V plot for the illuminated samples case. The efficiency (η) is the maximum produced power at operating point to incident light power fraction and given by[58].

$$\eta = \frac{I_{max} V_{max}}{p_{in}} * 100\% \quad \text{.....(3–4)}$$

CHAPTER FOUR

RESULTS & DISCUSSIONS

4-1 Introduction

This chapter includes results and discussions of X-ray diffraction, optical properties and FTIR measurements for pure and Cu doped ZnO nanoparticles prepared with different dopant ratio (0, 2, 4, 6 and 8%). Also this chapter includes solar cells parameters results for these samples with iodine on Si wafer.

4-2 X-Ray Diffraction

Figs. (4-1 to 4-5) show the matching of X-ray diffraction for pure and Cu doped ZnO nanoparticles, prepared with different dopant ratio (0, 2, 4, 6 and 8%), with ZnO standard lines Wurtzite Structure. These figures show poly crystalline structure with well-matched peaks corresponding to (100), (002), (101), (012), (110), (013) and (004) planes for hexagonal ZnO structure with standard card number (96-901-1663). These results agree with the [61].

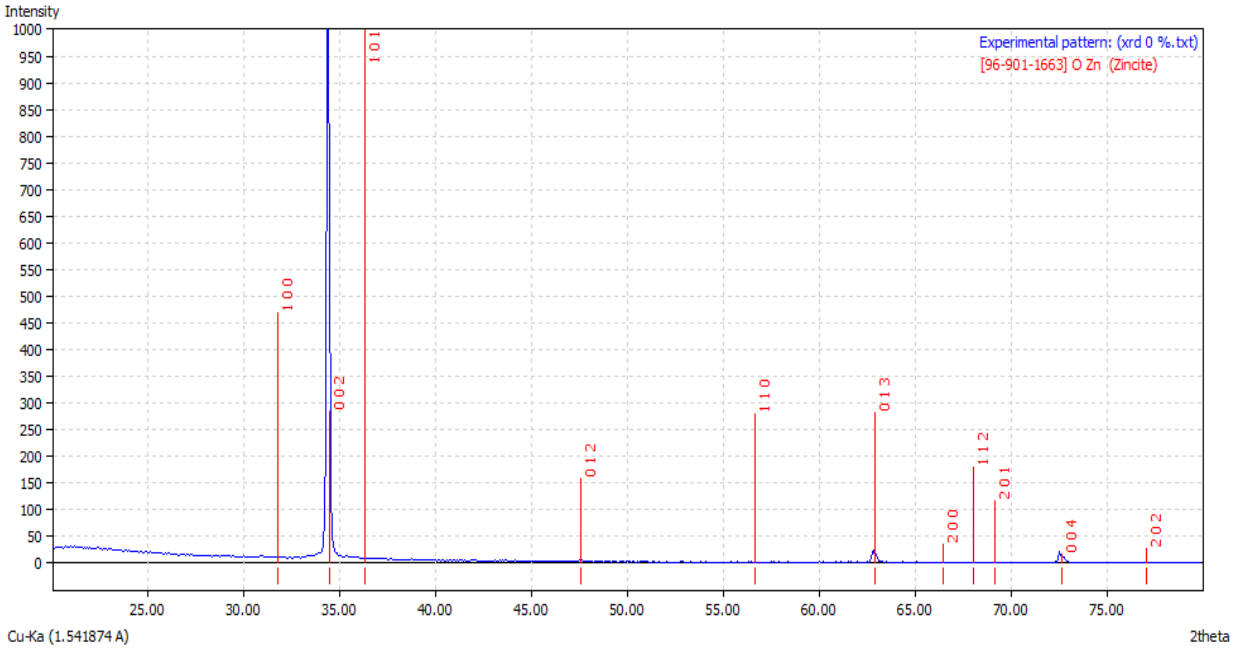

Fig. 4-1: Matching the XRD pattern for pure ZnO nanoparticles with standard lines

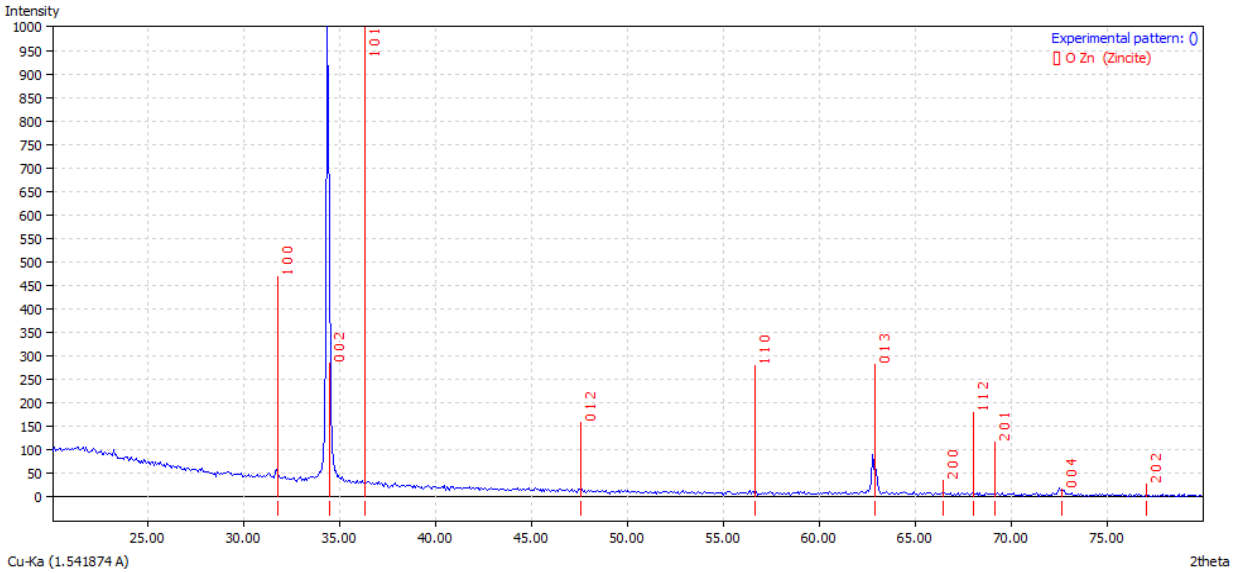

Fig. 4.2: Matching the XRD pattern for 2% Cu doped ZnO NPs with standard lines

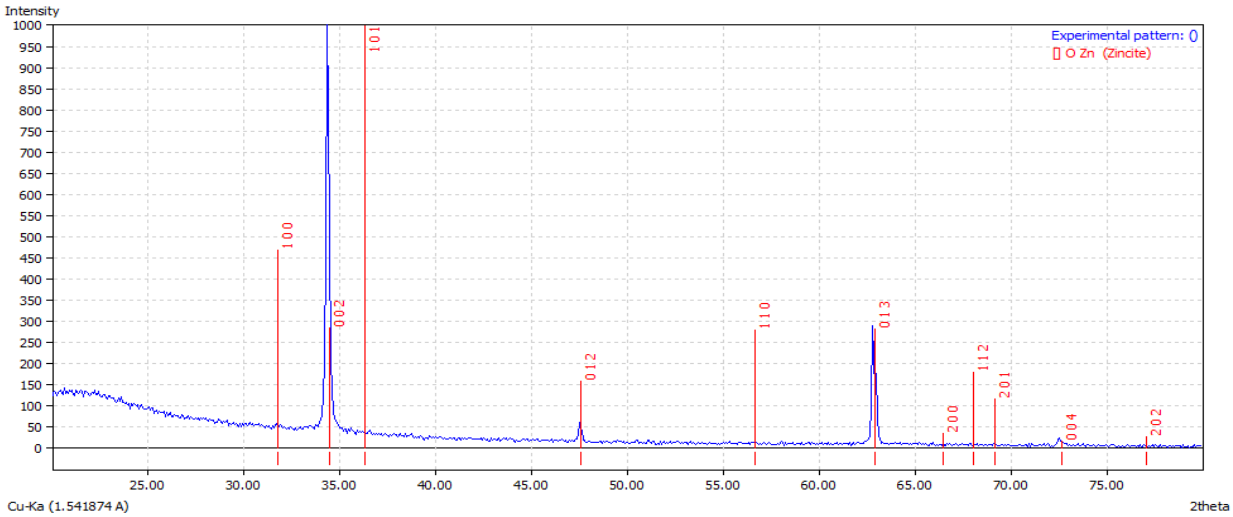

Fig. 4.3: Matching the XRD pattern for 4% Cu doped ZnO NPs with standard lines

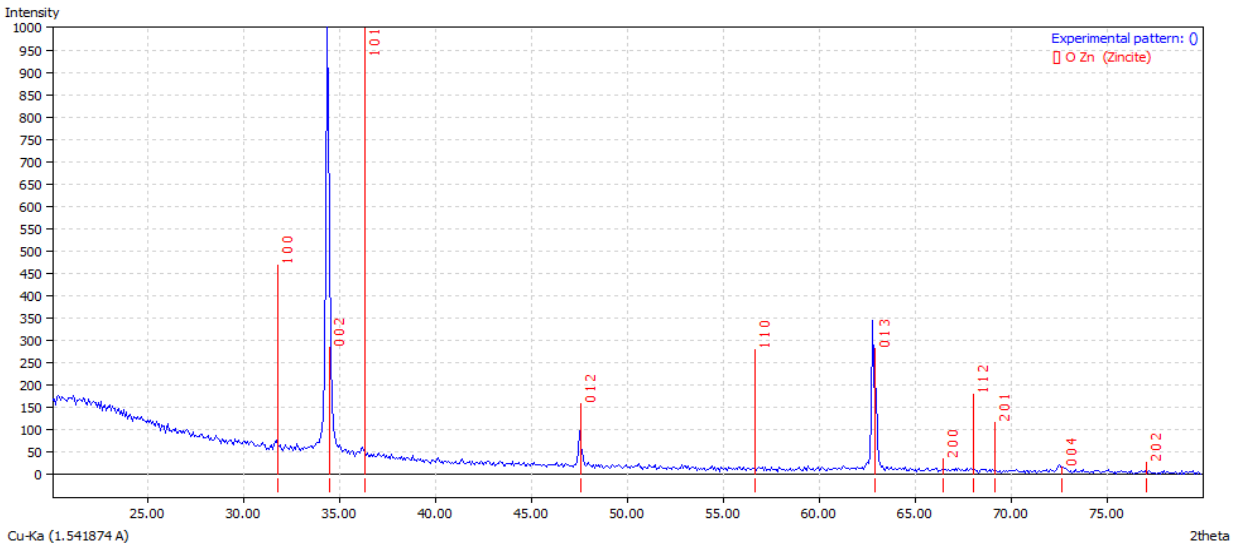

Fig. 4.4: Matching the XRD pattern for 6% Cu doped ZnO NPs with standard lines

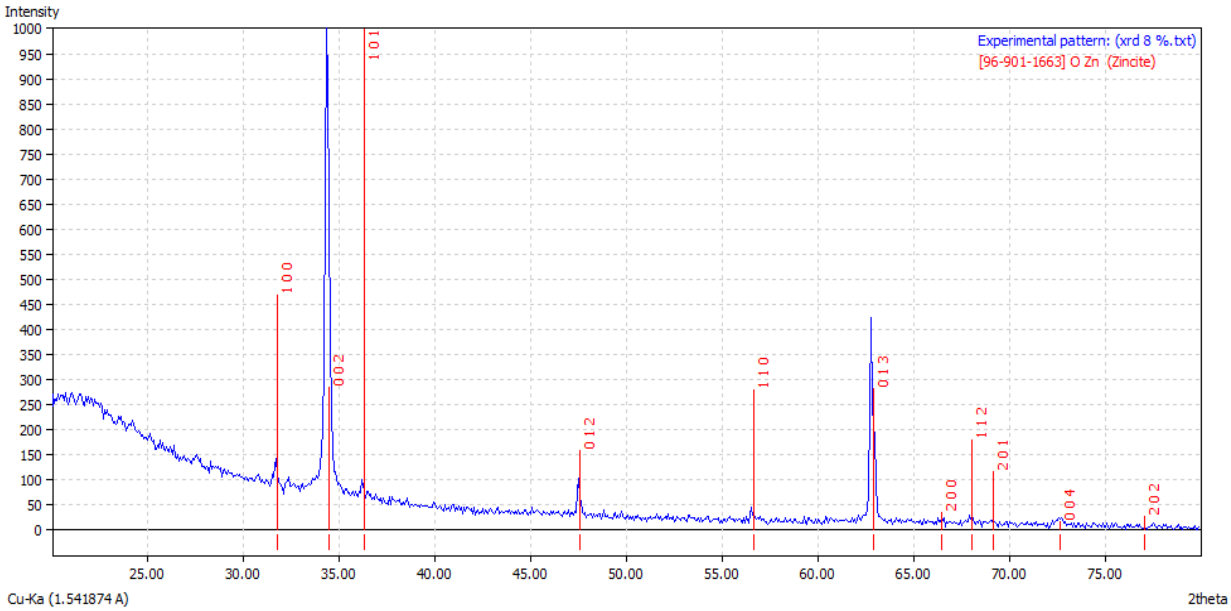

Fig. 4.5: Matching the XRD pattern for 8% Cu doped ZnO NPs with standard lines

Fig. (4.6) shows the planes representation of the clearest peaks in XRD {(002), (013) and (004)} for the prepared nanoparticles.

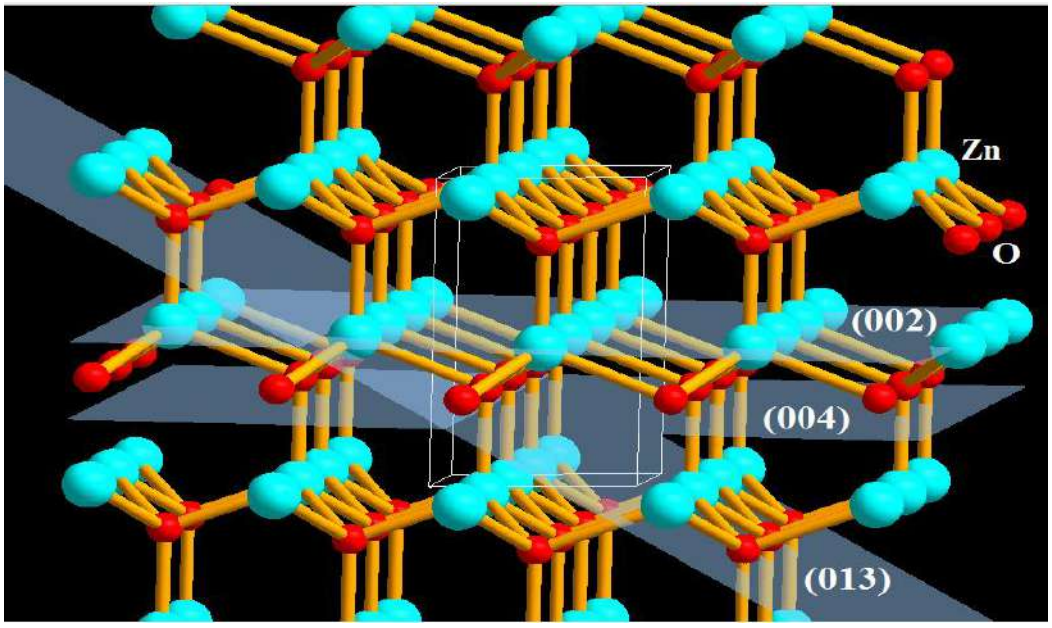

Fig. 4.6: Representing the planes of the clearest peaks in XRD (002), (013) and (004)

Fig. (4-7) shows a comparison between the X-ray diffraction patterns for pure and Cu doped ZnO nanoparticles prepared with different dopant ratio. It can be seen that the preferred orientation along (002) direction with intensity decrease with increasing doping ratio

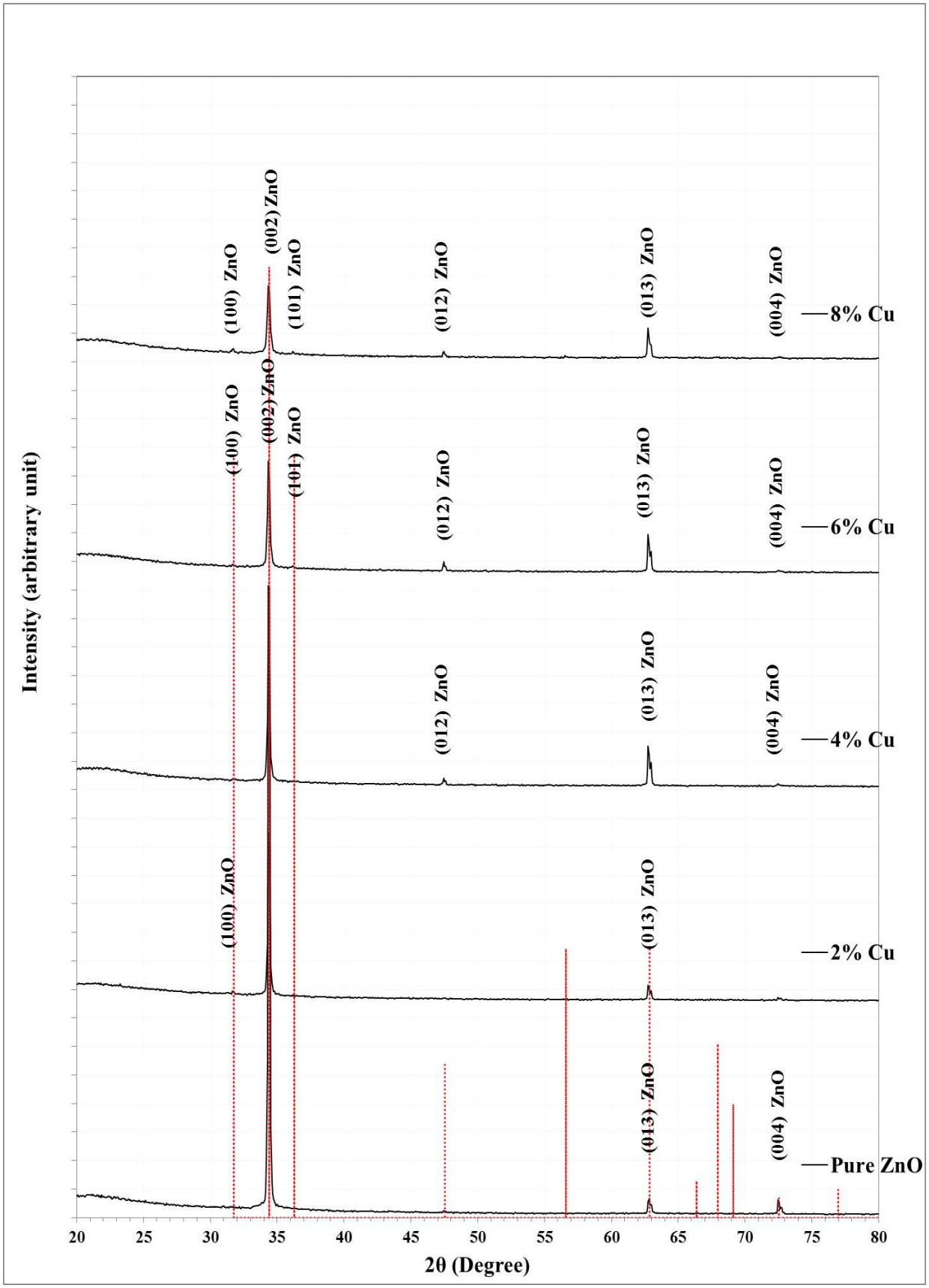

Fig. 4.7: XRD patterns for pure and Cu doped ZnO NPs with different ratio

Fig. (4-8) show the Gaussian fitting for all XRD peaks for pure and Cu doped ZnO NPs with different ratio using Xpowder software which done after removing the background.

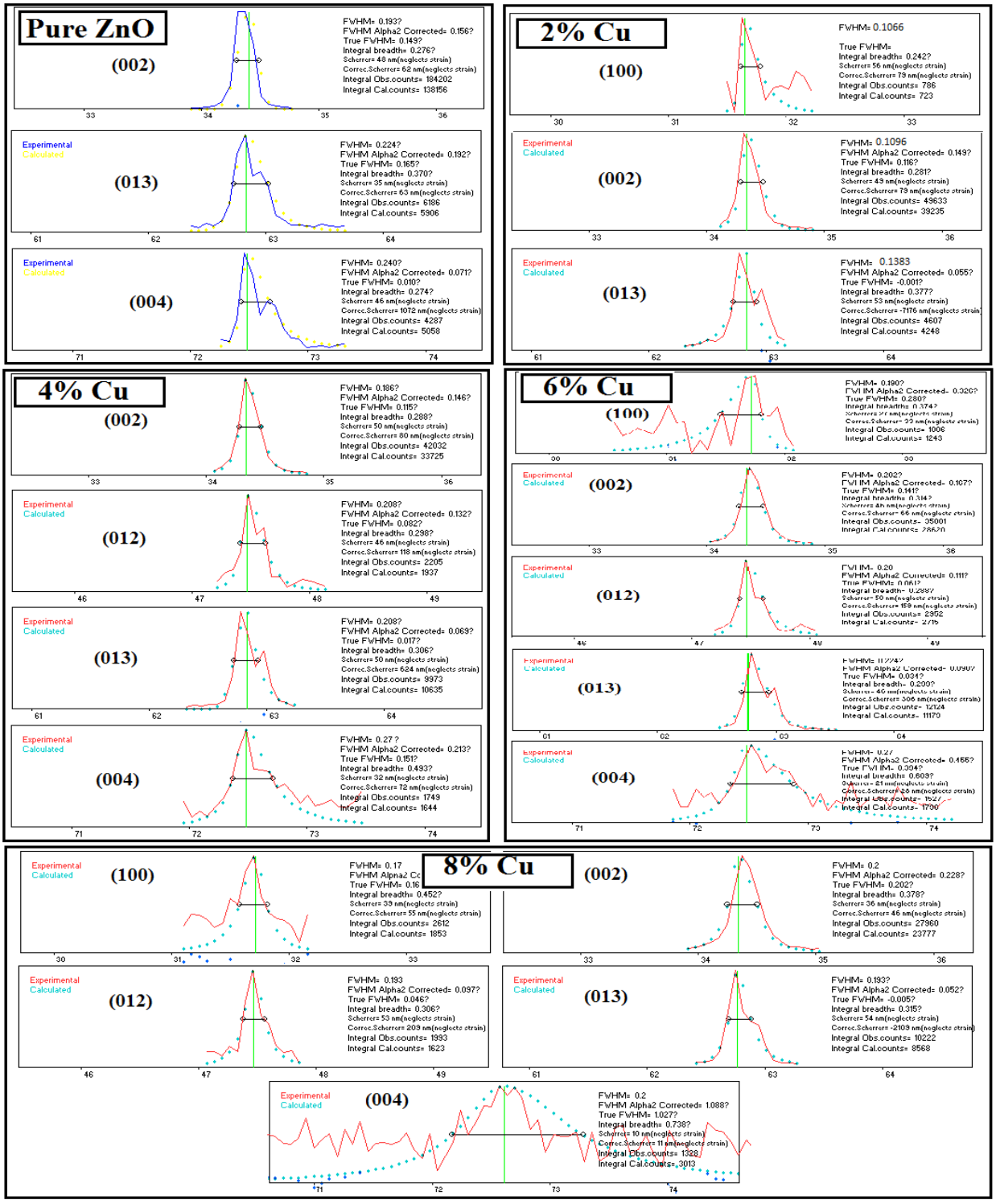

Fig. 4.8:Gaussian fitting for all XRD peaks for pure and Cu doped ZnO NPs with different ratio

Table (4-1) shows the Structural parameters, for pure and Cu doped ZnO NPs powder with different ratio, which contain Bragg angle (2θ) , full width at half maximum (FWHM), experimental inter-planar spacing (calculated using Bragg's low) compare with their standard values, crystalline size (calculated using Sherrer's formula) and the corresponding planes. This Table shows that the crystalline size increase at 2% Cu ratio and decrease with more ratio.

Table 4.1: 2θ, FWHM, experimental and standard d_{hkl} and the crystalline size for pure and Cu doped ZnO NPs with different ratio

Sample	2θ (Deg.)	FWHM (Deg.)	d_{hkl} Exp.(Å)	G.S (nm)	hkl	d_{hkl} Std.(Å)	Phase	Card No.
Pure ZnO	34.4050	0.1933	2.6046	43.0	(002)	2.6035	Hex. ZnO	96-901-1663
	62.8320	0.2245	1.4778	41.5	(013)	1.4772	Hex. ZnO	96-901-1663
	72.4820	0.2405	1.3030	41.0	(004)	1.3017	Hex. ZnO	96-901-1663
2% Cu	31.6480	0.1066	2.8249	77.5	(100)	2.8137	Hex. ZnO	96-901-1663
	34.3400	0.1096	2.6093	75.9	(002)	2.6035	Hex. ZnO	96-901-1663
	62.7660	0.1383	1.4792	67.3	(013)	1.4772	Hex. ZnO	96-901-1663
4% Cu	34.3400	0.1855	2.6093	44.8	(002)	2.6035	Hex. ZnO	96-901-1663
	47.4690	0.2080	1.9138	41.7	(012)	1.9110	Hex. ZnO	96-901-1665
	62.8320	0.2076	1.4778	44.9	(013)	1.4772	Hex. ZnO	96-901-1663
	72.4820	0.2710	1.3030	36.4	(004)	1.3017	Hex. ZnO	96-901-1663
6% Cu	31.7140	0.1940	2.8192	42.6	(100)	2.8137	Hex. ZnO	96-901-1663
	34.3400	0.2025	2.6093	41.1	(002)	2.6035	Hex. ZnO	96-901-1663
	36.1780	0.2000	2.4809	41.8	(101)	2.4754	Hex. ZnO	96-901-1663
	47.4690	0.2032	1.9138	42.7	(012)	1.9110	Hex. ZnO	96-901-1665
	62.7660	0.2335	1.4792	39.9	(013)	1.4772	Hex. ZnO	96-901-1663
	72.4820	0.2700	1.3030	36.5	(004)	1.3017	Hex. ZnO	96-901-1663
8% Cu	31.7140	0.1700	2.8192	48.6	(100)	2.8137	Hex. ZnO	96-901-1663
	34.3400	0.2000	2.6093	41.6	(002)	2.6035	Hex. ZnO	96-901-1663
	36.1780	0.2200	2.4809	38.0	(101)	2.4754	Hex. ZnO	96-901-1663
	47.4690	0.1932	1.9138	44.9	(012)	1.9110	Hex. ZnO	96-901-1665
	62.7660	0.1932	1.4792	48.2	(013)	1.4772	Hex. ZnO	96-901-1663
	72.6130	0.2010	1.3010	49.1	(004)	1.3017	Hex. ZnO	96-901-1663

Fig. (4.9) shows the Williamson and Hall plot for the XRD peaks, the relation between $\beta cos\theta$ (β in radians) against 4 sinθ, with the best linear fitting with their equations. The slope represent the non-uniform strain in lattice, while

the grain size calculated using equation (2-2) and equal to ($0.9*0.15406/y_{intersection}$) [nm].

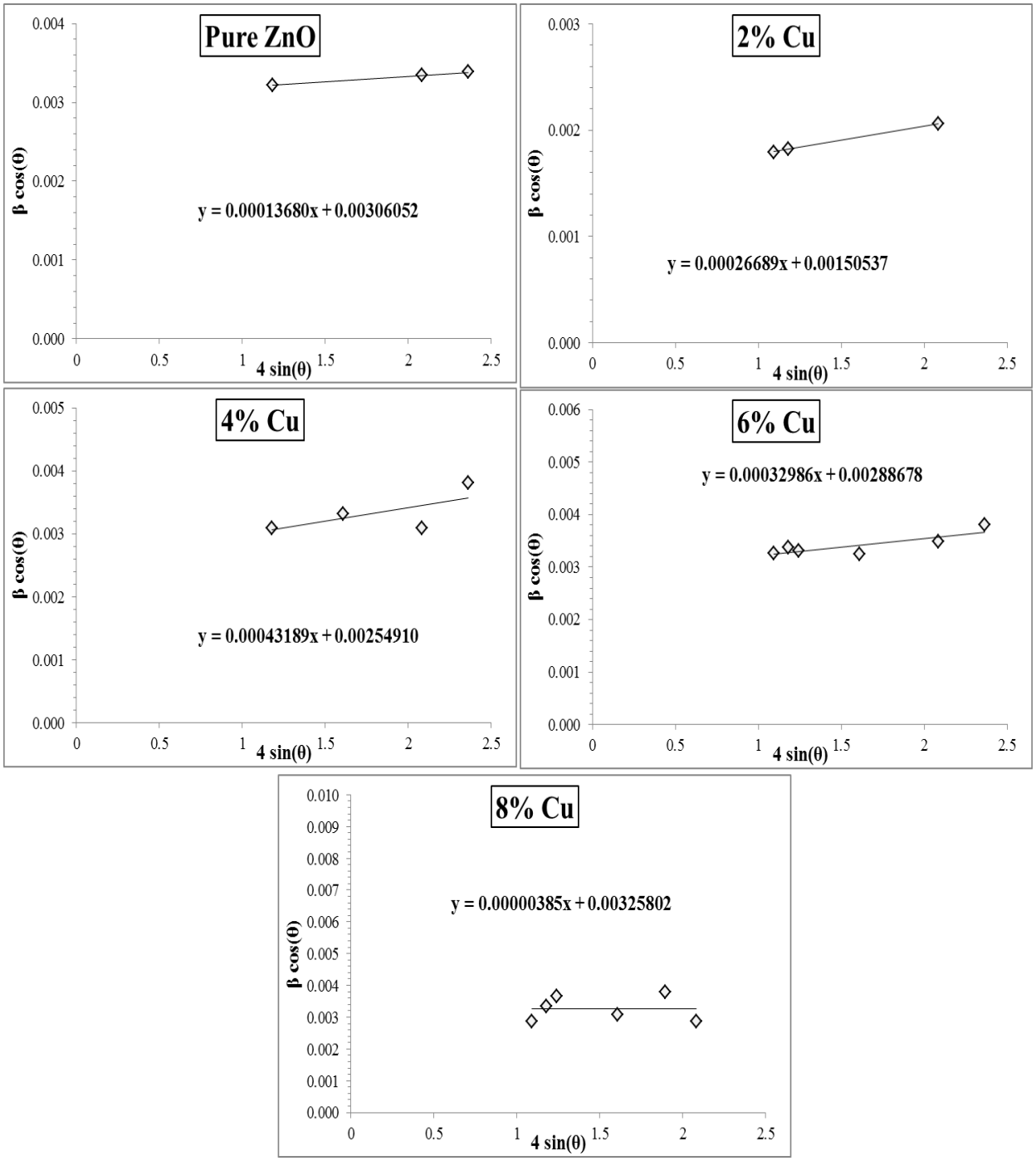

Fig. 4.9: W-H plot for XRD patterns corresponding to pure and Cu doped ZnO NPs with different ratio

Fig. (4.10) shows the variation of grain size (D), calculated by Williamson-Hall plot for the prepared nanoparticles, with the copper dopant ratio. This figure shows that the maximum value for D at 2% Cu then decrease with increasing doping ratio.

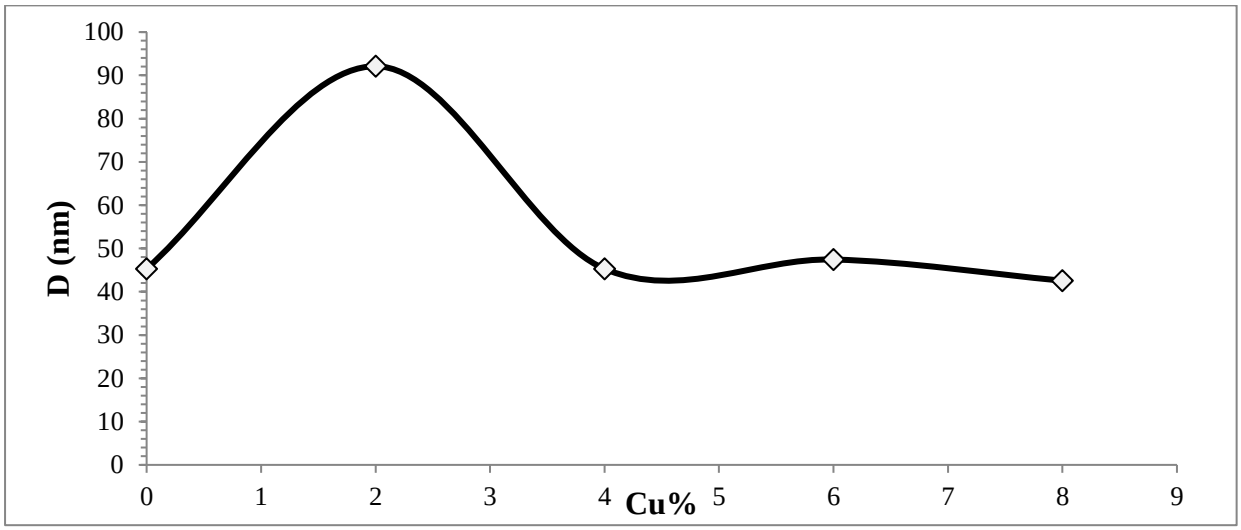

Fig. 4.10: Variation of the grain size calculated by W-H plot for pure and Cu doped ZnO NPs with different ratio

Fig. (4.11) shows the variation of non-uniform strain (ε), calculated by Williamson-Hall plot, with the Cu ratio. This figure shows that (ε) increase with increasing Cu ratio specially at 8% as a result of increasing lattice defects.

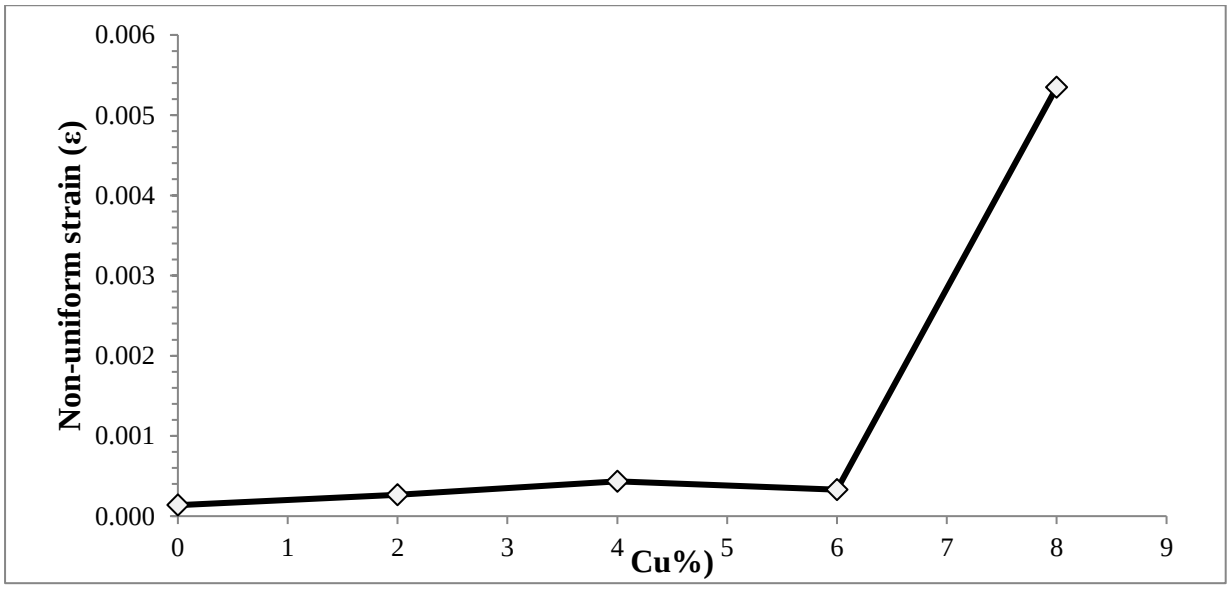

Fig. 4.11: Variation of the non-uniform strain calculated by W-H plot for pure and Cu doped ZnO NPs with different ratio

Fig. (4.12) shows the two dimensional representation for the XRD pattern for ZnO with different doping ratio. This figure concentrates on (002) and (013) peaks. It show how the peaks locations shifted to less values, i.e. increase the d_{hkl} values for these planes with increasing Cu content in sample.

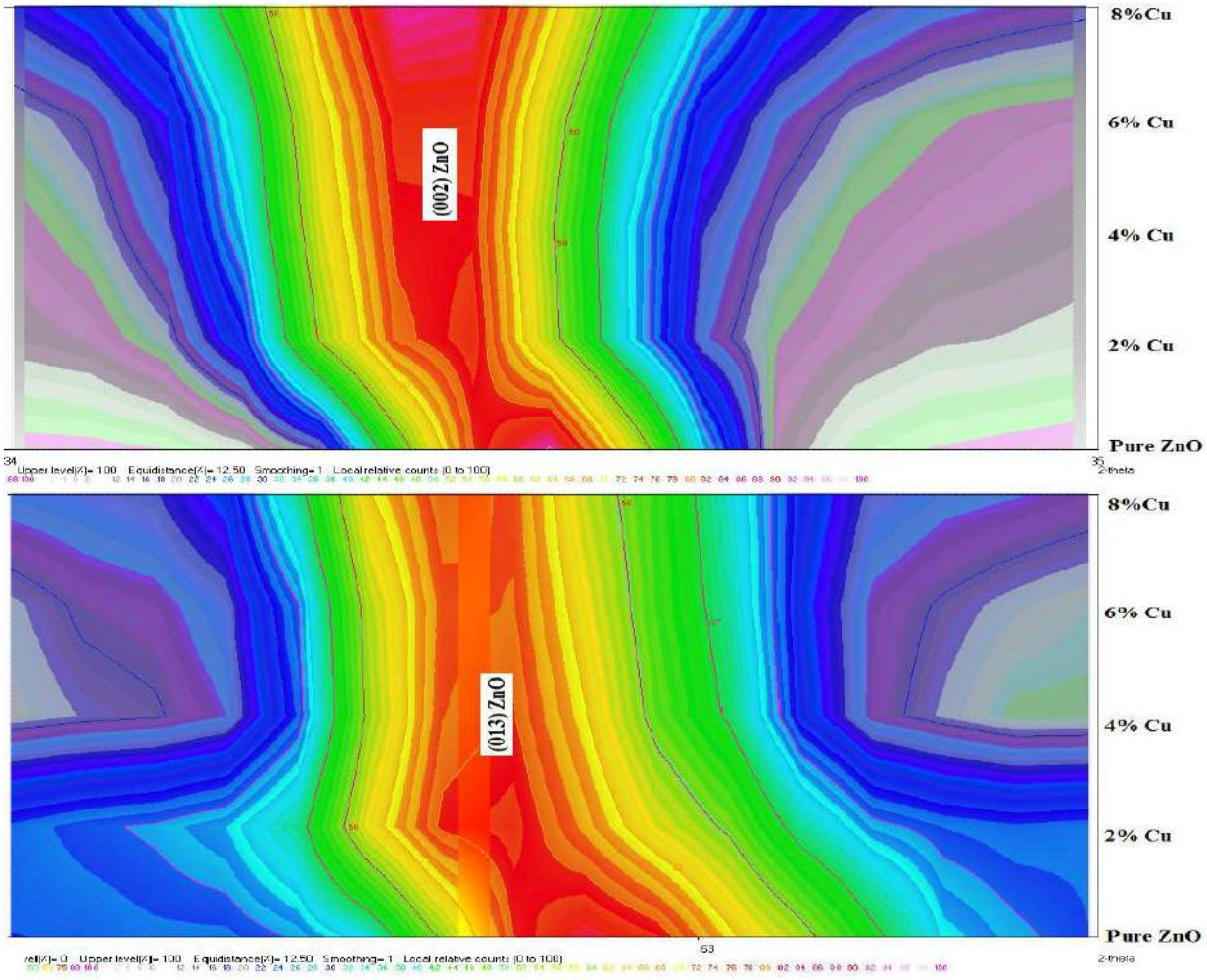

Fig. 4.12: Two-dimensional XRD representation for Cu doped ZnO with different doping ratio, focus on (002) and (013)

Lattice parameters (a and c for hexagonal structure) were calculated using the equation $\frac{1}{d^2} = \frac{4}{3}\frac{h^2+hk+k^2}{a^2} + \frac{l^2}{c^2}$ using the (002) and (013) direction (clear peaks and exist in all patterns). Table (4.2) show the lattice constants, non-uniform strain and the grain size calculated by W-H method for all ZnO samples doped with different ratio with copper.

Table (4.2) : Lattice constants non uniform strain and the grain size calculated by W-H method for pure and Cu doped ZnO samples with different ratio.

Cu%	a (Å)	c (Å)	Non uniform strain	W-H grain size
0	3.250110	5.209134	0.000137	45.30407
2	3.255220	5.212808	0.000267	92.10626
4	3.249388	5.215750	0.000432	45.30407
6	3.247996	5.217223	0.000330	47.45142
8	3.245600	5.218696	0.005350	42.55801

Fig. (4.13 and 4.14) show the variation of lattice constants (a and c) for hexagonal structure. These figures illustrate that (a) increase at 2% Cu ratio then decrease with more ratio, while (c) increase with increasing Cu ratio, maybe due to the variation in grain size.

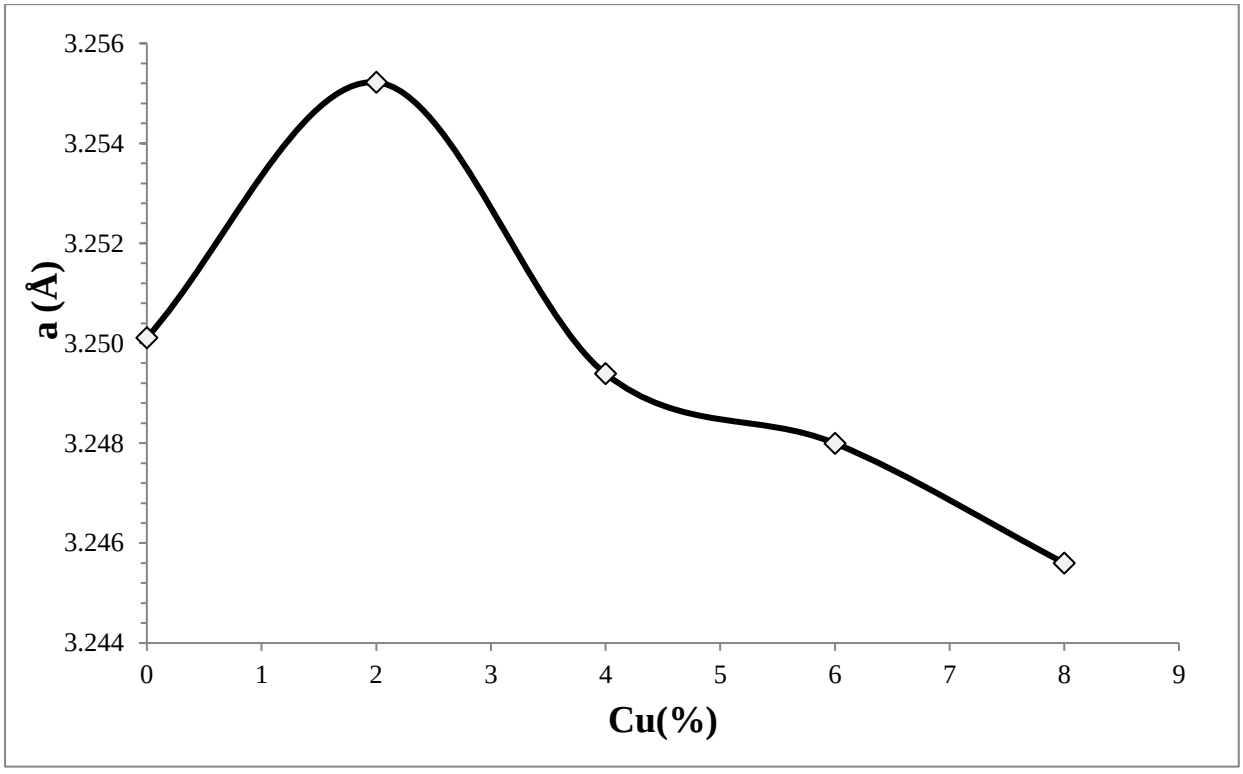

Fig. 4.13: Variation of lattice constant (a) with Cu ratio

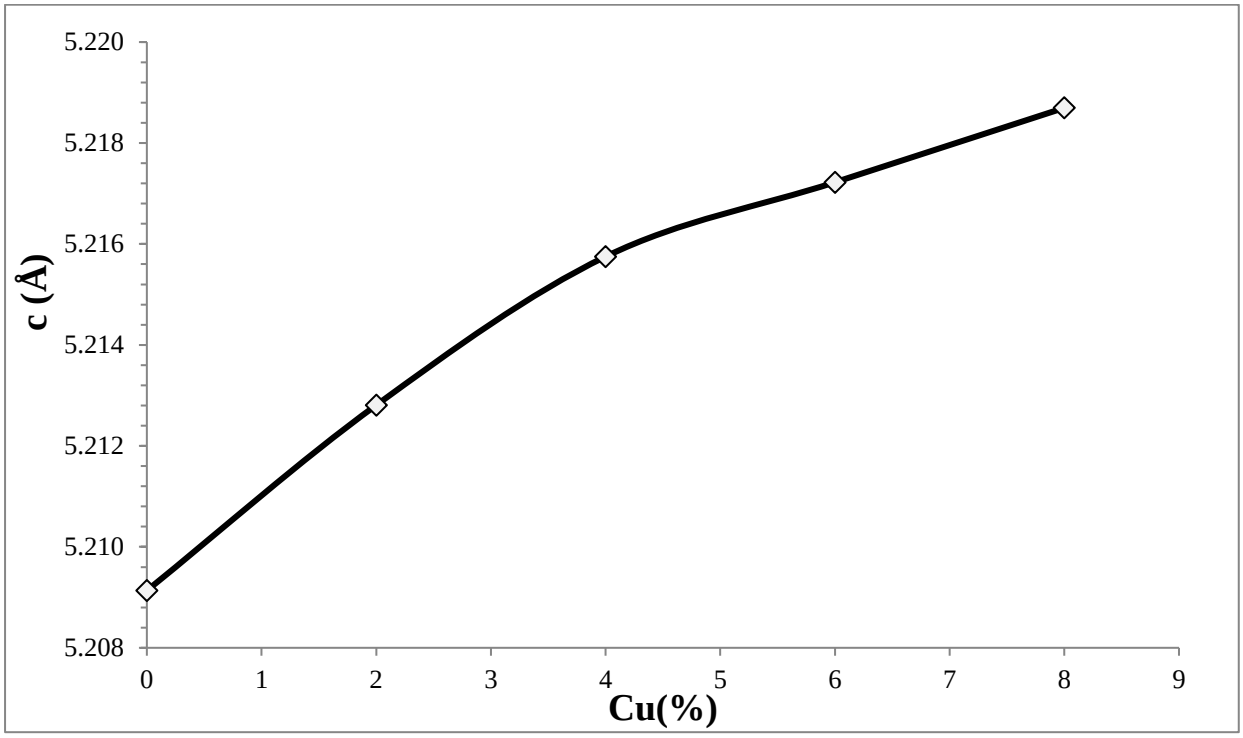

Fig. 4.14: Variation of lattice constant (c) with Cu ratio

4-3 Optical properties

From UV-Visible absorption, the optical measurements for pure and Cu doped ZnO nanoparticles suspension in water with different Cu ratio are carried out in the wavelength range 350–750 nm.

4-3-1 Transmittance Spectra

Fig. (4.15) shows the transmittance spectra for pure and Cu doped ZnO nanoparticles at different Cu ratio. In general, it can be observed that the transmittance increases with increasing the wavelength, for all prepared samples. The transmittance increases with increasing doping ratio to 8% reaching values higher than 90% in the visible region. There is a sharp fall in the transmittance for doped samples, which is due to the strong absorbance of the films in this region.

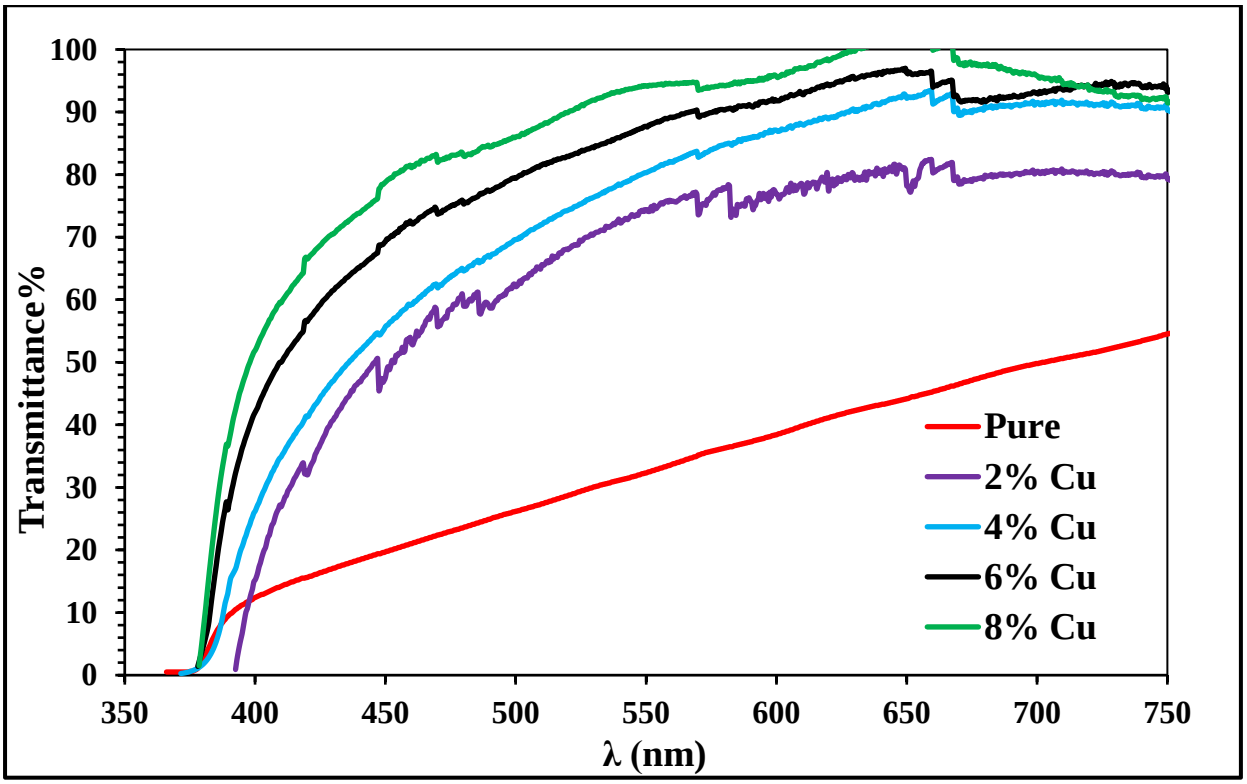

Fig. 4.15: The variation of transmission with wavelength for pure and Cu doped ZnO suspension with different doping ratio

4-3-2 Optical Energy Gap

The optical energy gap values (E_g^{opt}) for pure and Cu doped ZnO nanoparticles at different Cu ratio have been determined by using Tauc equation, By plotting the relation of $(\alpha h\upsilon)^2$ versus photon energy ($h\upsilon$). Linear dependence, which describes all films have allowed direct transition. The optical energy gap (E_g^{opt}) is then determined from the point of intersection between line tangent and x-axis as shown in Fig. (4-16) for different Cu ratio.

It can be observe that the increasing of Cu content from 0 to 2% leads to decrease the optical band gap from 3.20 to 3.14 eV and then increase to 3.26 eV at 8% Cu due to decreasing the nanoparticle as a result of quantum effect for nansize particles.

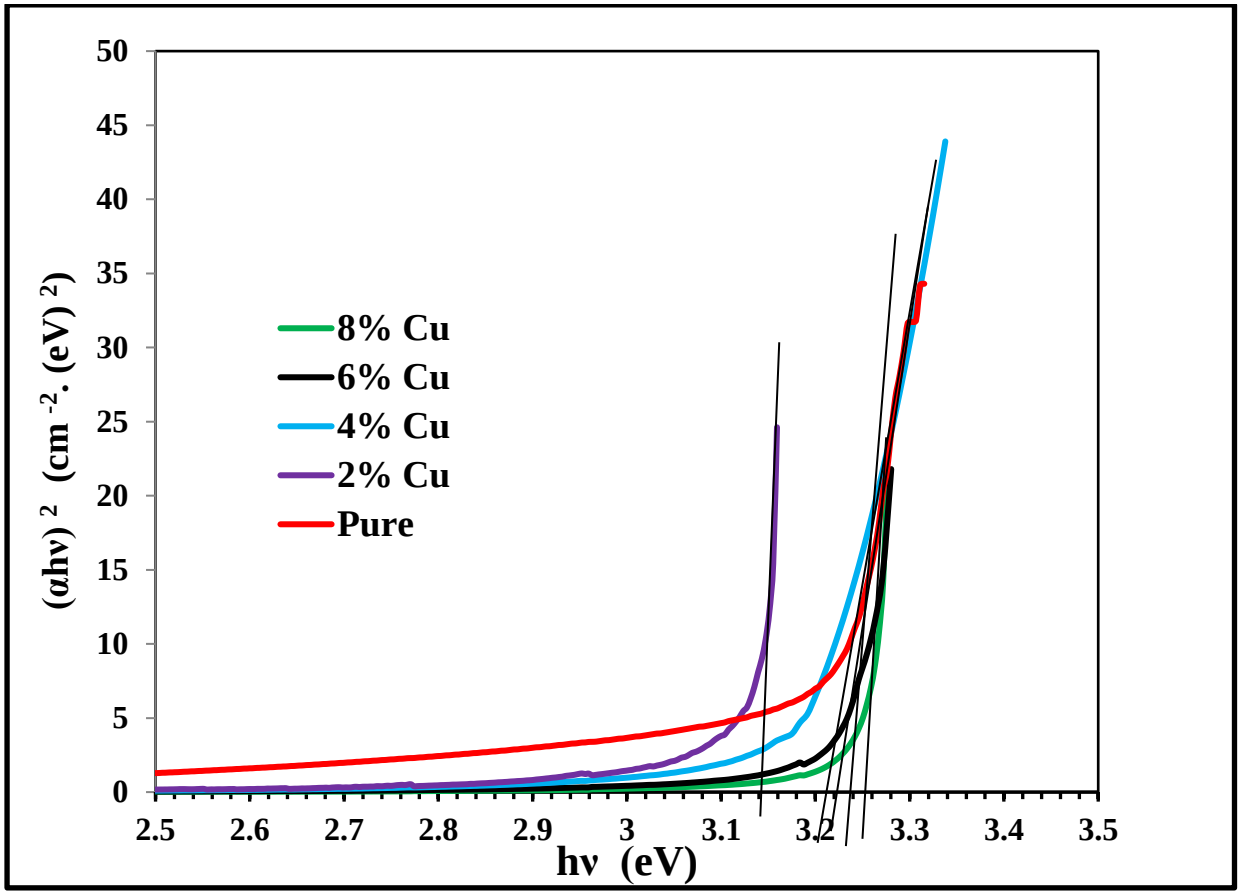

Fig. 4-16: The variation of $(\alpha h\upsilon)^2$ versus photon energy ($h\upsilon$) for pure and Cu doped ZnO suspension with different doping ratio

4-3-3 Extinction Coefficient

Fig.(4.17) shows the variation of extinction coefficient (k) with wavelength for pure and Cu doped ZnO nanoparticles at different Cu ratio. The extinction coefficient depends mainly on absorption coefficient; for this reason it has the same behavior.

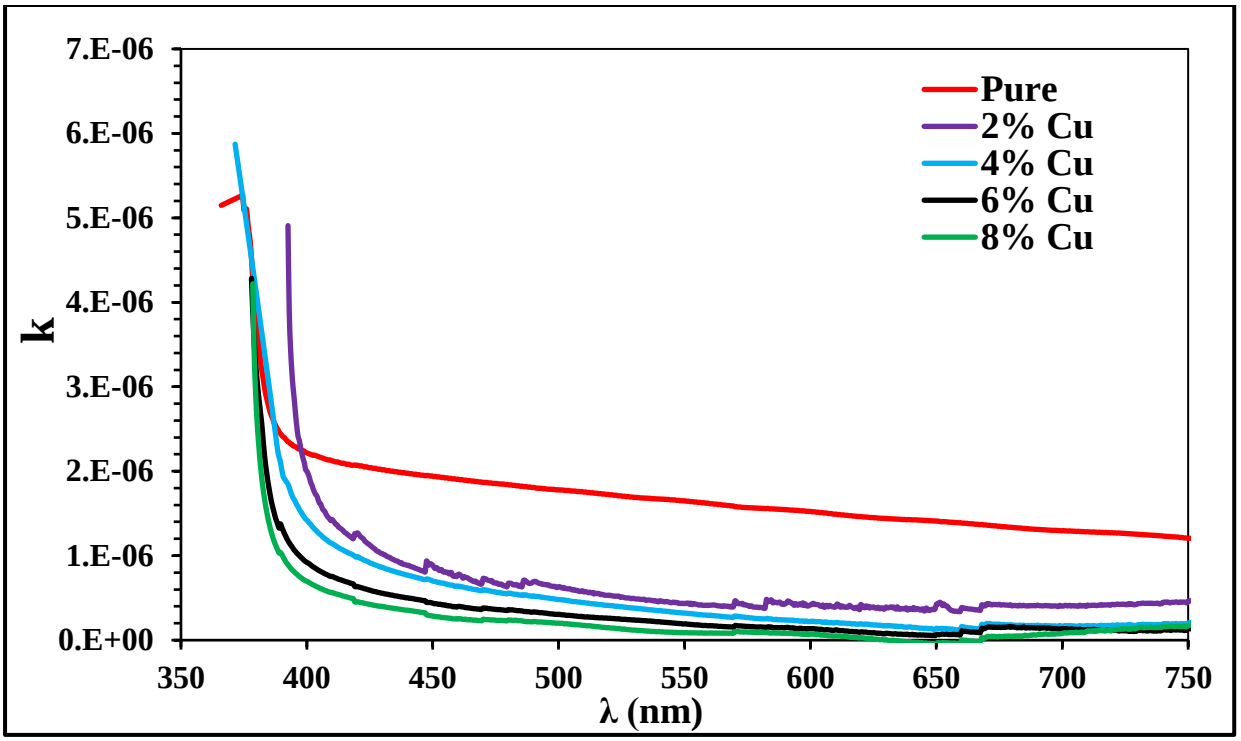

Fig. 4.17: The variation of extinction coefficient with wavelength for pure and Cu doped ZnO suspension with different doping ratio

4-3-4 Refractive Index

The variation of the refractive index versus wavelength in the range 350–750 nm, for pure and Cu doped ZnO nanoparticles at different Cu ratio were shown in Fig. (4.18). It has been noticed that the refractive index in general decreases with increasing of Cu content maybe due to the variation of surface morphology.

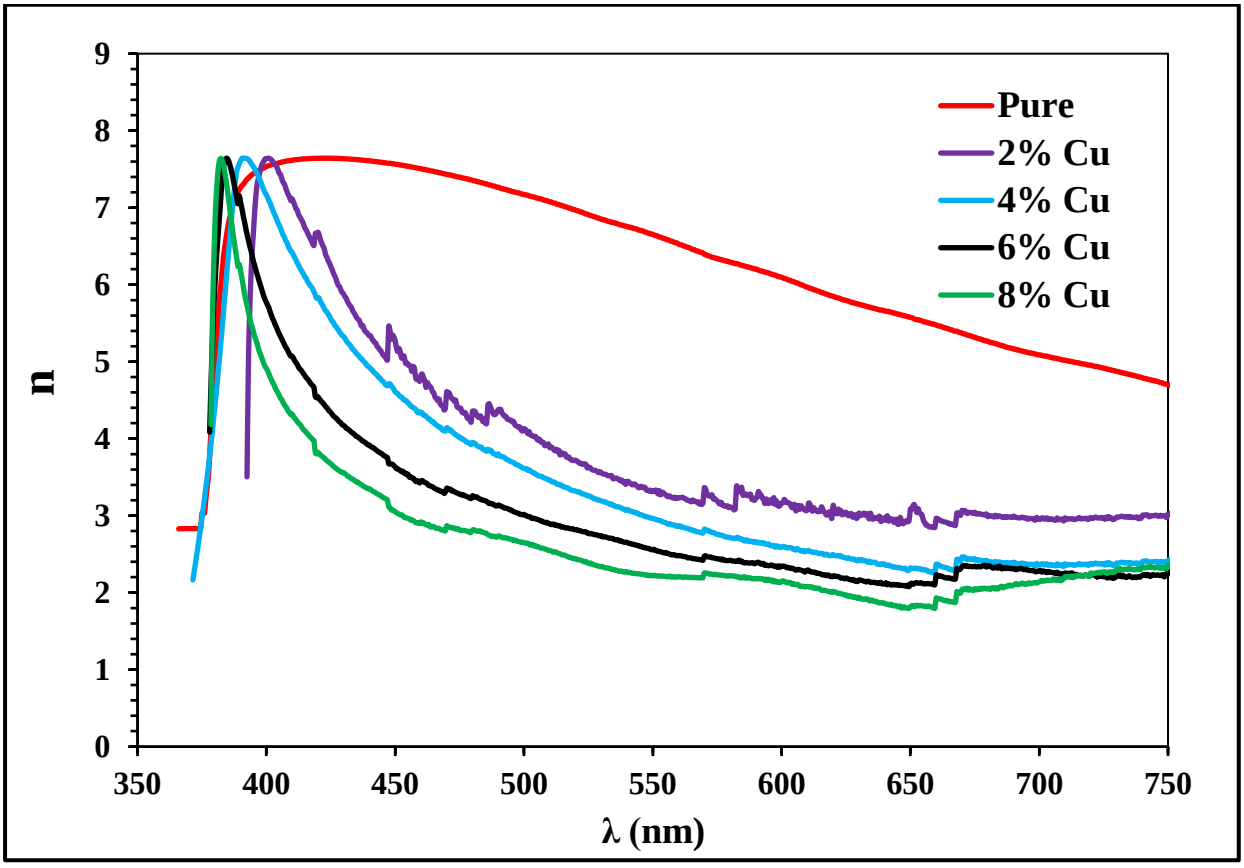

Fig. 4.18: The variation of refractive index with wavelength for pure and Cu doped ZnO suspension with different doping ratio

4-3-5 The Dielectric Constants

The variation of the real and imaginary parts of the dielectric constant values versus wavelength have been shown in figures (4.19 and 4.20) for pure and Cu doped ZnO nanoparticles at different Cu ratio . The variation of the dielectric constant depends on the value of the refractive index. By contrast, the dielectric loss depends mainly on the extinction coefficient values which are related to the variation of absorption, so have nearly same behavior.

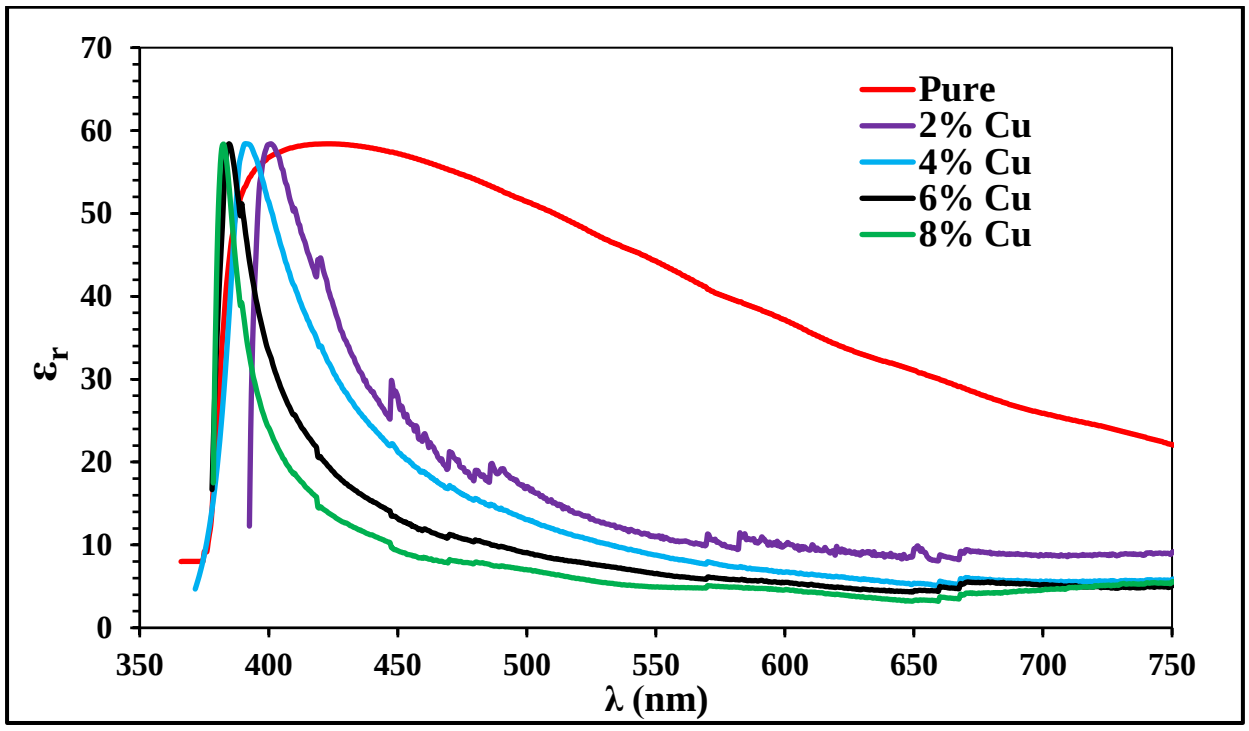

Fig. 4.19: The variation of ε_r with wavelength for pure and Cu doped ZnO suspension with different doping ratio

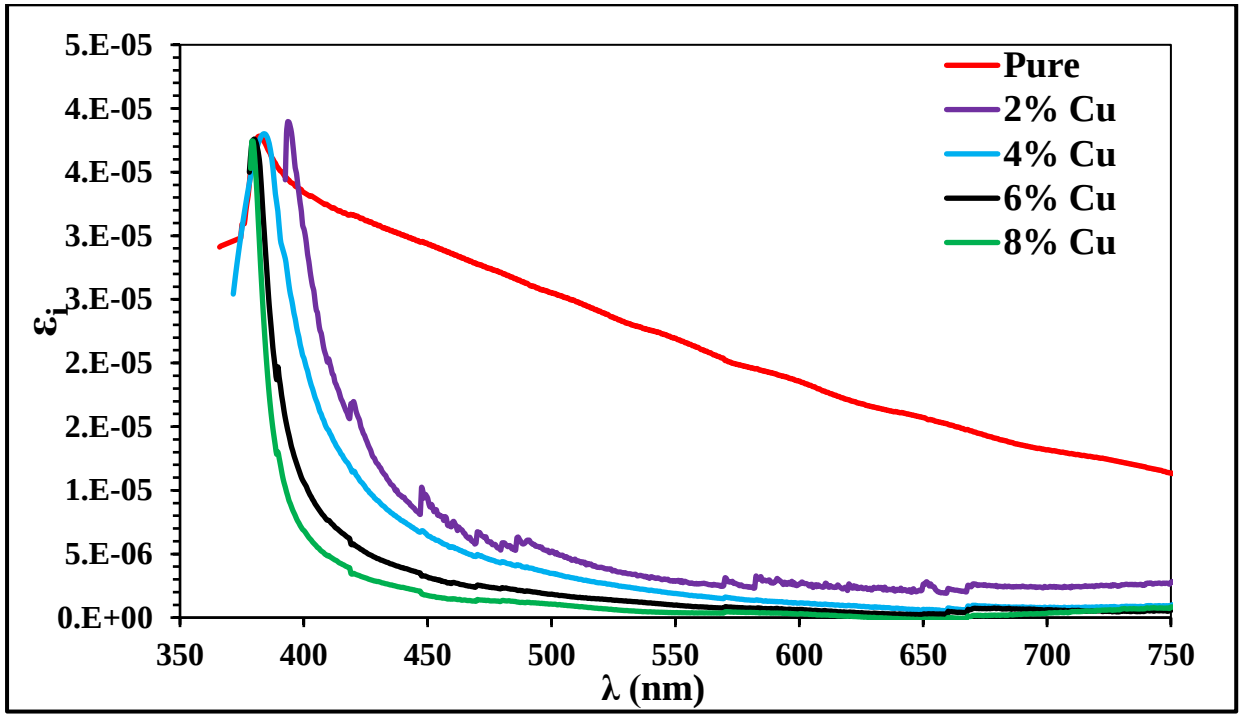

Fig. 4.20: The variation of ε_i with wavelength for pure and Cu doped ZnO suspension with different doping ratio

Table (4-3) shows the optical constants for pure and Cu doped ZnO suspension with different doping at λ=550 nm and the energy gap values for these samples.

Table 4-5: optical constants at λ=550 nm and $E_g^{Opt.}$ for pure and Cu doped ZnO suspension with different doping ratio

Cu%	T%	α (cm^{-1})	K	n	ε_r	ε_i	Eg (eV)
0	32.30	0.377	1.65E-06	6.654	44.282	2.20E-05	3.20
2	74.20	0.099	4.36E-07	3.325	11.057	2.90E-06	3.14
4	80.30	0.073	3.20E-07	2.964	8.788	1.90E-06	3.18
6	87.70	0.044	1.92E-07	2.558	6.542	9.80E-07	3.24
8	94.20	0.020	8.72E-08	2.220	4.928	3.87E-07	3.26

4-4 FTIR Measurements

Fig. (4.21) Shows the FTIR patterns for Cu doped ZnO with different ratios (2, 4, 6 and 8)%. This figure shows many peaks at nearly same locations corresponding to O-H, C-H, S-H, C=C and C-O bonds comes from the adsorbed gasses on surface of sample. Another sharp peaks located at 1384 cm^{-1} corresponding to $ZnCO_3$ attachment. Small peaks located in the range from 420 to 620 cm^{-1} corresponding to Zn-O vibrations, indicate on ZnO formation. All observed peaks were shown in Table (4-4).

Table 4-6: observed peaks in FTIR patterns for Cu doped ZnO NPs with different ratio

	2% Cu	4% Cu	6% Cu	8% Cu
Zn-O stretch	466.03 617.59	454.02 617.59	466.03 619.09	421.01 452.52 472.03 616.09
C-O stretch	1033.26 1106.79	1027.26 1111.30	1031.76 1105.29	1028.76 1106.79
$ZnCO_3$	1384.41	1384.41	1384.41	1384.41
C=C	1636.52	1636.52	1635.01	1635.01
S-H	2352.31	2352.31	2353.81	2352.31
C-H stretch	2852.02 2919.55	2852.02 2922.55	2850.52 2921.05	2852.02 2928.55
O-H	3465.78	3449.27	3443.27	3440.27

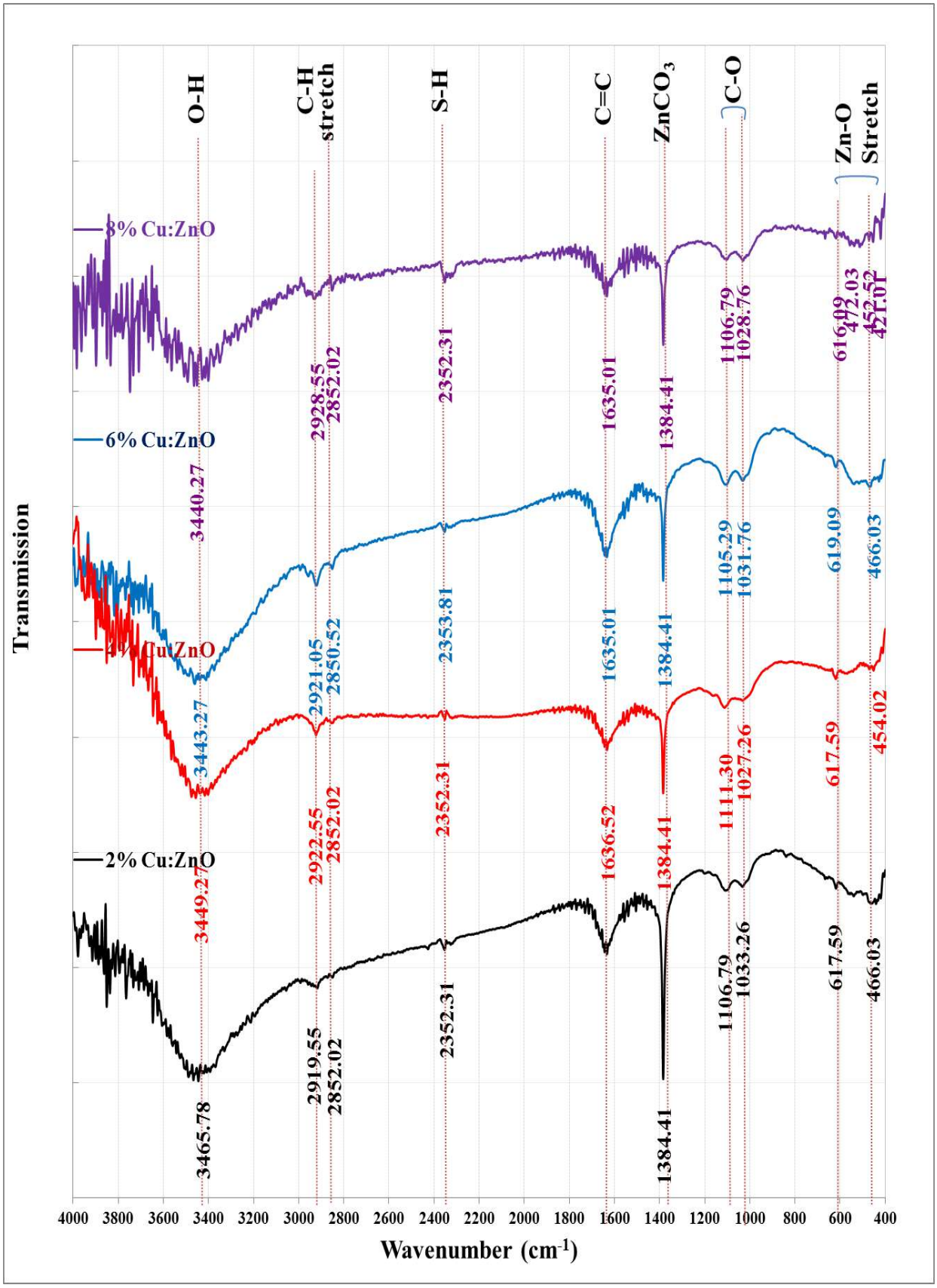

Fig. 4.21: FTIR patterns for Cu doped ZnO with different ratios (2, 4 and 6)%.

4-5 Current-Voltage Characteristics for DSSC

In order to determine the performance of fabricated dye solar cell, as well as its electrical behavior, current-voltage (I-V) measurements under illumination are performed.

The I-V characteristics for DSSC under illumination using power densities equal to 550 mW/cm^2 with the applied forward bias for samples produced by Cu doped ZnO NPs with different ratio (2, 4, 6 and 8) at % were shown in Figs. (4.22 to 4.25).

The solar cells parameters such as: V_o, I_{sc}, I_m, V_m, FF and the solar cell efficiency were calculated from these figures as shown in Table (4-7). This Table shows that the efficiency increase with increasing the Cu dopant ratio reach to 0.0439 at 8% Cu content

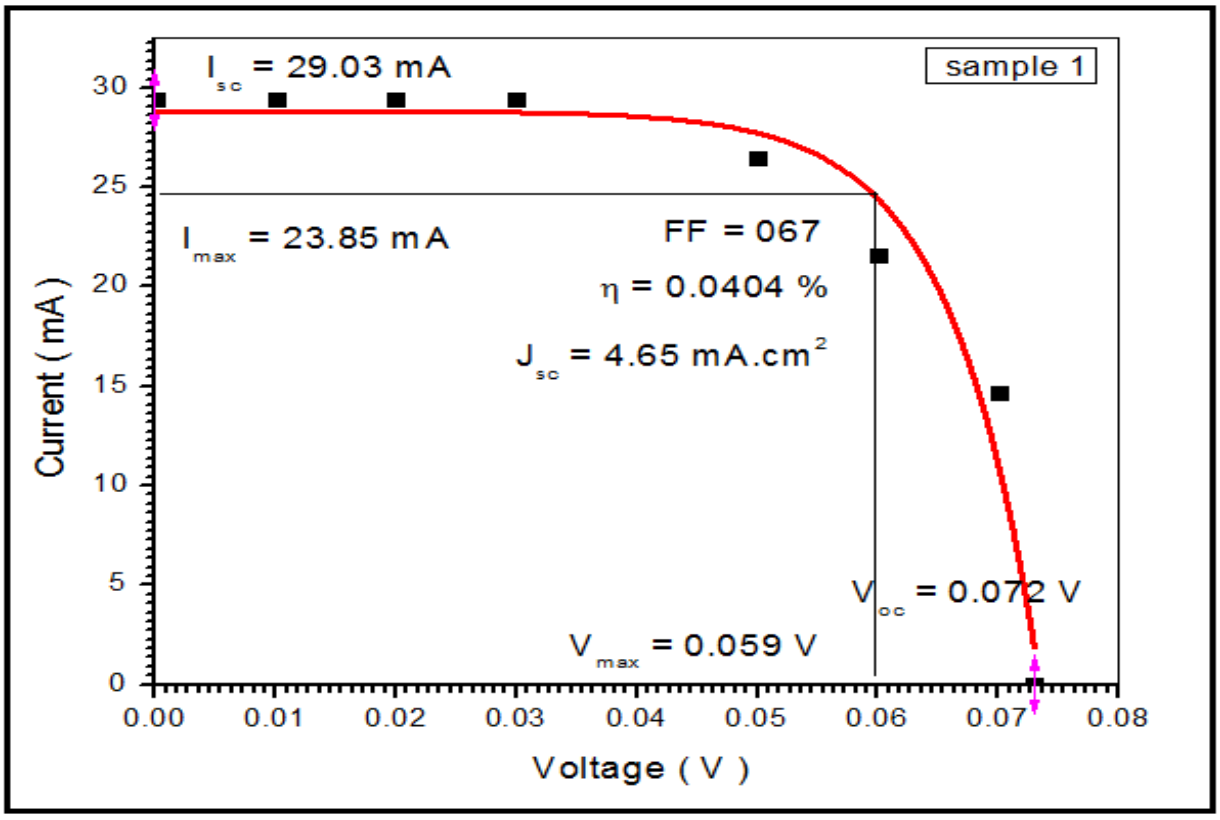

Fig. 4.22: I-V characteristics for DSSC based on Cu doped ZnO with 2% Cu

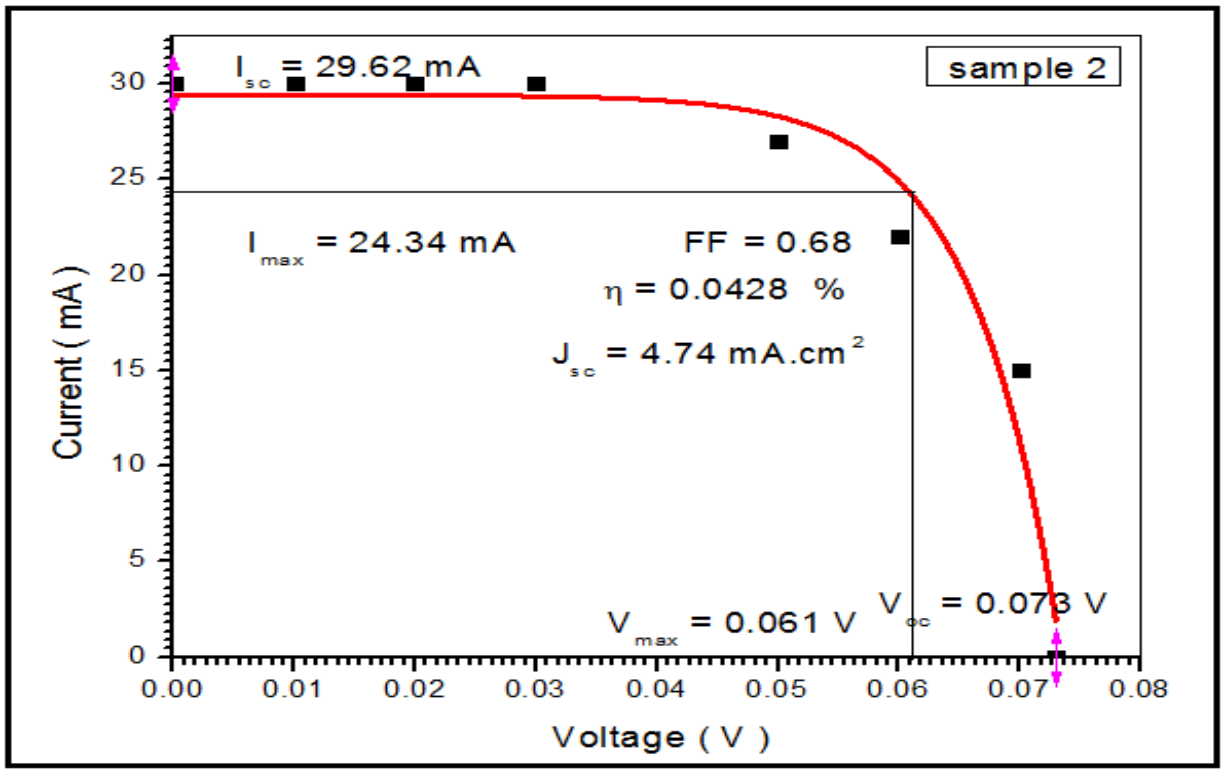

Fig. 4.23: I-V characteristics for DSSC based on Cu doped ZnO with 4% Cu

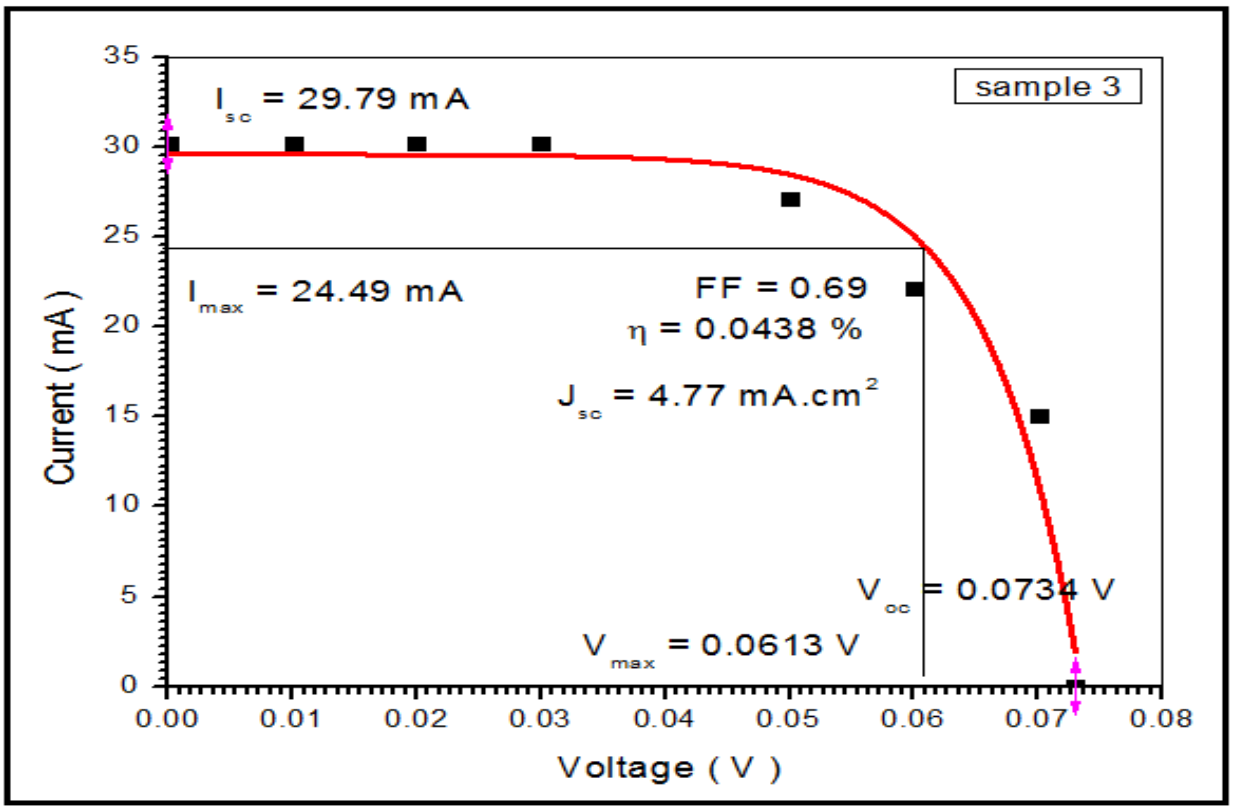

Fig. 4.24: I-V characteristics for DSSC based on Cu doped ZnO with 6% Cu

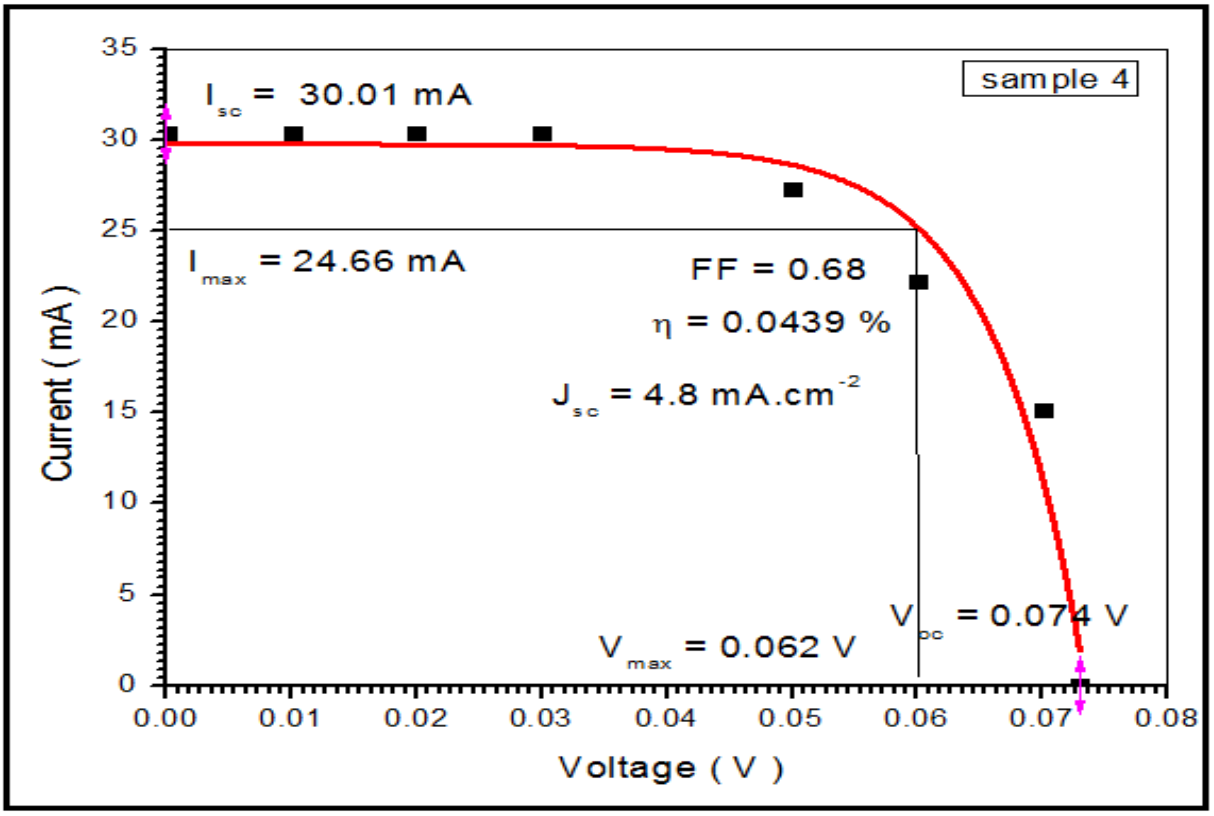

Fig. 4.25: I-V characteristics for DSSC based on Cu doped ZnO with 8% Cu

Table (4-7) solar cell Parameters for DSSC based on Cu doped ZnO with different ratios

Cu%	I_{sc} (mA)	V_{oc} (V)	I_m (mA)	V_m(v)	F.F	η%
2	29.0300	0.0720	23.8500	0.0590	0.6732	0.0404
4	29.6200	0.0730	24.3400	0.0610	0.6867	0.0408
6	29.7900	0.0734	24.4900	0.0613	0.6866	0.0438
8	30.0100	0.0740	24.6600	0.0620	0.6885	0.0439

CHAPTER FIVE

CONCLUSIONS

Conclusions

Study the characteristics of pure and Cu doped ZnO nanoparticles with different ratios prepared by hydro thermal method shows many points as follows:

The X-ray diffraction shows poly crystalline structure for all samples, identical with standard peaks. Increasing Cu ratio leads to decrease the preferred orientation peak intensity along (002) direction. The crystalline size, calculated by Sherrer formula, increase at 2% Cu ratio and decrease with more ratio. The grain size calculated by W& H equation increase from 45.30 to 92.10 nm with 2% Cu then decrease with more ratio to 42.56 nm at 8% Cu ratio, while the non-uniform strain increase, with increasing Cu ratio from 0 to 8% .

The optical properties for produced NPs show that the transmission spectra increases with increasing Cu ratio to reach about 90%. The optical energy gap obey relation for r=1/2 (allowed direct transition) . Increasing of Cu content from 0 to 2% leads to decrease the optical band gap from 3.20 to 3.14 eV, while more ratio cause to increase to 3.26 eV at 8% Cu .

FTIR measurements indicate the formation of ZnO compound.

The solar cells measurements show that the efficiency increase with increasing the Cu dopant ratio.

Suggestion for Future Works

1- Doing another measurements such as Scanning electron microscopy and electrical properties (DC conductivity with temperature and Hall effect measurements)

2- Use the prepared nanoparticles in another application such as gas sensor or photo detector.

3- Using another types of doping such as the rare earth metals

REFERENCES

References

[1] A. Jha, *Solar Cell Technology and Applications*. USA: CRC press Taylor& Francis Group, 2010.

[2] Dye-Sensitized vs. Thin Film Solar Cells", European Institute for Energy Research, 30 June 2006.

[3] Brian O'Regan; Michael Grätzel 'A low-cost, high-efficiency solar cell based on dye-sensitized colloidal TiO2 films'. Nature. 353 (6346): 737–740, 1991.

[4] D. Wei, "Dye Sensitized Solar Cells," *Int. J. Mol. Sci.*, vol. 11, pp. 1103–1113, 2010.

[5] A. Patil, C. Dighavkar, and R. Borse, "Al doped ZnO thick films as CO 2 gas sensors," *J. Optoelectron. Adv. Mater.*, vol. 13, no. 10, pp. 1331–1337, 2011.

[6] H. Tributsch 'Dye sensitization solar cells: a critical assessment of the learning curve'. Coordination Chemistry Reviews. 248 (13–14): 1511–1530, 2004.

[7] M. Pagliaro, G. Palmisano, and R. Ciriminna, *Flexible solar cells*. Weinheim: WILEY-VCH Verlag GmbH & Co. kGaA, 2004.

[8] H. Gerischer, M. Michel-Beyerle, E. Rebentrost, H. Tributsch, 'Sensitization of Charge-Injection into Semiconductors with Large Band Gap'. Electrochimica Acta. Vol. 13 , No.6,PP.1509–1515, 1968.

[9] M. Matsumura,S. Matsudaira, H. Tsubomura, M. Takata, H. Yanagida 'Dye Sensitization and Surface Structures of Semiconductor Electrodes'. Ind. Eng. Chem. Prod. Res. Dev. Vol. 19 , No.3, PP. 415–421, 1980.

[10] M. Mukhtar, L. Munisa, and R. Saleh, "Co-Precipitation Synthesis and Characterization of Nanocrystalline Zinc Oxide Particles Doped with Cu_2+ Ions," *Mater. Sci. Appl.*, vol. 3, pp. 543–551, 2012.

[11] C. Bhakat and P. P. Singh, "Zinc Oxide Nanorods : Synthesis and Its Applications in Solar Cell," vol. 2, no. 4, pp. 2452–2454, 2012.

[12] C. Justin, K. Prabakar, S. N. Karthick, K. V Hemalatha, M. Son, and H. Kim, "Banyan Root Structured Mg-Doped ZnO Photoanode Dye-Sensitized Solar Cells," *Am. Chem. Soc.*, vol. 117, pp. 2600–2607, 2013.

[13] C. Hsu, C. Lai, L. Chen, and P. Chan, "Enhanced Performance of Dye-Sensitized Solar Cells with Graphene / ZnO Nanoparticles Bilayer Structure," *J. Nanomater.*, vol. 2014, no. 3, pp. 1–7, 2014.

[14] J. T. Illakkiya, S. Hemalatha, R. Oommen, and P. U. Rajalakshmi, "Characterization of ZnO Nanoparticles synthesized by wet chemical method," *Int. J. ChemTech Res.*, vol. 6, no. 3, pp. 2159–2161, 2014.

[15] M. Jyoti, D. Vijay, and S. Radha, "To Study the Role of Temperature and Sodium Hydroxide Concentration in the Synthesis of Zinc," *Int. J. Sci. Res. Publ.*, vol. 3, no. 11, pp. 2–6, 2013.

[16] D. Ahmed, M. Osman, and M. A. Mustafa, "Synthesis and

Characterization of Zinc Oxide Nanoparticles using Zinc Acetate Dihydrate and Sodium Hydroxide Synthesis and Characterization of Zinc Oxide Nanoparticles using Zinc Acetate Dihydrate and Sodium Hydroxide," no. January, 2016.

[17] N. A. Salahuddin, M. El-kemary, and E. M. Ibrahim, "Synthesis and Characterization of ZnO Nanoparticles via Precipitation Method : Effect of Annealing Temperature on Particle Size," vol. 5, no. 4, pp. 82–88, 2015.

[18] R. Sadraei, "A Simple Method for Preparation of Nano-sized ZnO," *Res. Rev. J. Chem.*, vol. 5, no. 2, pp. 45–49, 2016.

[19] D. R. Lide, "CRC Handbook of Chemistry and Physics," *Handb. Chem. Phys.*, vol. 53, no. 84th Edition, 2003.

[20] A. Ashrafi and C. Jagadish, "Review of zincblende ZnO: Stability of metastable ZnO phases," *J. Appl. Phys.*, vol. 102, no. 7, 2007.

[21] Y. Xu and W. Ching, "Electronic, optical, and structural properties of some wurtzite crystals," *Phys. Rev. B*, vol. 48, pp. 4335–4351, 1993.

[22] V. Coleman and C. Jagadish, "Basic Properties and Applications of ZnO," in *Zinc Oxide Bulk, Thin Films and Nanostructures*, no. December, Elsevier Limited, 2006, p. Ch1.

[23] Pearton, S. J., Norton, D. P., Ip, K., Heo, Y. W., and Steiner, T., Recent progress in processing and properties of ZnO. Progress in Materials Science, 50(3):p. 293-340, 2005. .

[24] M. L. T. Cossio *et al.*, *Biosensing using Nanomaterials*, vol. XXXIII, no. 2. 2012.

[25] K.R,Murali ″Properties of sol-gel dip-coated zinc oxide thin films″, Journal of Physics and Chemistry of Solids, Vol. 68No.12, pp. 2293-2296, 2007.

[26] K. S. Karimov *et al.*, "Ag / PEPC / NiPc / ZnO / Ag thin film capacitive and resistive humidity sensors," vol. 31, no. 5, pp. 1–6, 2010.

[27] A. S. H. Hameed *et al.*, "In vitro antibacterial activity of ZnO and Nd doped ZnO nanoparticles against ESBL producing Escherichia coli and Klebsiella pneumoniae," *Sci. Rep.*, vol. 6, no. 1, p. 24312, 2016.

[28] G. Modi, "Zinc oxide tetrapod : a morphology with multifunctional applications," *Nanosci. Nanotechnol*, vol. 6, pp. 1–8, 2015.

[29] I. Linkov and J. Steevens, *Nanomaterials. Risks and Benefits*. USA: Springer, 2009.

[30] A. Kołodziejczak-radzimska and T. Jesionowski, "Zinc Oxide—From Synthesis to Application: A Review," pp. 2833–2881, 2014.

[31] Y. Gogotsi, *Nanomaterials Handbook*. Boca Raton: Taylor & Francis Group CRC press, 2006.

[32] M. Quintana,T. Edvinsson, A. Hagfeldt, G. Boschloo, Comparison of Dye-Sensitized ZnO and TiO2 Solar Cells: Studies of Charge Transport and Carrier Lifetime. J. Phys. Chem. C, Vol. 111, PP.1035–1041,2007.

[33] F. Group, *Nanotechnology in Biology and Medicine*. Boca Raton: CRC Press, 2006.
[34] C. Dupas P. Houdy M. Lahmani, *Nanoscience-Nanotechnologies and Nanophysics*, Springer. Verlag Berlin Heidelberg, 2007.
[35] K. Zho, *Nanoscience and nanotechnologies: opportunities and uncertainties*. UK: The Royal Society, 2004.
[36] W. H. Bragg and W. L. Bragg, *X Rays and Crystal Structure*. London: G. Bell and Sons, LTD., 1918.
[37] P. Scherrer, "Göttinger Nachrichten Gesell," vol. 2, p. 98, 1918.
[38] M. S. Dresselhaus, "Solid State Physics Part II: Optical Properties of Solids," *Proceedins Int. Sch. Phys.*, vol. 0, pp. 1–194, 2001.
[39] B. Ray, *II-VI Compounds*, 1st ed. Printed in GB, 1969.
[40] H. Fritzche, *Amorphous and Liquid Semiconductors*, Plenums pr. New York and London, 1974.
[41] R.A. Greiner, *Semiconductor Device*. McGraw-Hill Book Company, 1989.
[42] D. A. Newman, *Semiconductor Physics and Devices-Basis Principles*. USA: McGraw-Hill companies , Richard D. & Irwin, Inc., 1990.
[43] J. Millman, *Microelectronics*. Kogakusha: , McGraw-Hill Book Company, 1979.
[44] R. Elliot and A.I.Gibson, *An Introduction to Solid State Physics and Application*, 1st editio. Macillian Inc., 1974.
[45] M. H. Brodisky, *Amorphous Semiconductors*. Berlin Heidelberg: Springer-Verlage, 1979.
[46] N. Mottand and E. Davis, *Electronic Process in Non-Crystalline Materials*. Oxford University Press, 1980.
[47] R.A. Greiner, *Semiconductor Device*. Electronic Energy Series, McGraw-Hill Book Co. Inc., 1961.
[48] L. Kazmarski, *Polycrystalline and Amorphous Semiconductors and Devices*. Academic Press: Academic Press, 1980.
[49] L.Chopra, ″Thin Film Phenomena″, McGraw-Hill,Inc(1969).
[50] T.A.Mcmath , , Ph D .Thesis, Simon Fraser University (1978).
[51] H.A. Macleod, ″Thin Film Optical Filters ″, 3rd Edition , Institute of physics publishing ,2001.
[52] B.Ray, [II-VI Compounds], Pergamon Press, 1st edition printed, Great Britain , Ne and Co. Ltd. of Edinburgh, p.162, (1969).
[53] S. M. Sze and K. Kwok, *Physics of Semiconductor Devices*, 3rd Editio. USA: A john wiley & Sons, Inc, 2007.
[54] S. Elliott,'Physics of Amorphous Materials', Longman Inc. New York, Vol.155, p.p: 98, (1984).
[55] A.Lenk, B.Schultrich, and T.Witke, "Diagnostics of laser ablation and laser induced plasmas," *Appl. Surf. Sci.*, vol. 106, pp. 473–477, 1996.
[56] J. Singh, *Optical Properties of Condensed Matter and Applications*.

New Delhi, India: John Wiley & Sons, 2006.
[57] J. Nelson, *The Physics of Solar Cells (Properties of Semiconductor Materials)*, 1st Editio. UK: Imperial College Press, 2003.
[58] T. Aernouts, *Organic Bulk Heterojunction Solar Cells From Single Cells*. Belgie: IMEC, 2006.
[59] M. Green, "Accuracy of analytical expressions for solar-cell fill factor," *J. Appl. Phy.*, pp. 337–340, 1982.
[60] G. Sivaraman, "Characterization of Cadmium Zinc Telluride Solar Cells," University of South Florida, 2003.
[61] Y. Xu , W. Ching , 'Electronic, optical, and structural properties of some wurtzite crystals', Physical Review B 48, 4335-4351, 1993.

Appendix

X-ray diffraction standard card for hexagonal ZnO structure

Entry # 96-901-1663

Phase classification

Name	
Mineral Name	Zincite
Formula	ZnO
I/Ic	7.62
Sample Name	9011662
Quality	C (calculated)

References

Publication

Bibliography	Xu Y. N., Ching W. Y., "Electronic, optical, and structural properties of some wurtzite crystals", Physical Review B **48**, 4335-4351 (1993)

Origin of data

Source of entry	COD (Crystallography Open Database)
Link to orig. entry	9011662

Crystal structure

Crystallographic data

Space group	P 63 m c (186)
Crystal system	hexagonal
Cell parameters	a=3.2490 Å c=5.2070 Å

Atom coordinates

Element	**Oxid.**	***x***	***y***	***z***
Zn		0.667	0.333	0
O		0.667	0.333	0.345

Diffraction data

Diffraction lines

d [Å]	**Int.**	**h**	**k**	**l**	**Mult.**
2.8137	470.5	1	0	0	6
2.6035	287.4	0	0	2	2
2.4754	1000	1	0	1	12
1.911	160.5	0	1	2	12
1.6245	282.6	1	1	0	6
1.4772	284.3	0	1	3	12
1.4069	38.7	2	0	0	6
1.3782	183.1	1	1	2	12
1.3582	119.3	2	0	1	12
1.3017	20.7	0	0	4	2
1.2377	29.3	2	0	2	12
1.1814	21	0	1	4	12
1.0929	80.8	0	2	3	12
1.0635	24.6	2	1	0	12
1.042	86.5	2	1	1	24
1.0158	50.2	1	1	4	12

جامعة النيلين
كلية الدراسات العليا
قسم الفيزياء

Cu Doped ZnO as Transparent Electrode for DSSC

من قبل
خمائل ابراهيم عبد الواحد

إشراف

مصباح حميد بابكر

1439هجري

2017 ميلادي